RAL
Laboratory
Appleton Laboratory

**RAL Report**
RAL-94-095

**CONTRIBUTIONS TO**

# EPAC 94

# LONDON

4th EUROPEAN PARTICLE ACCELERATOR CONFERENCE
EUROPHYSICS CONFERENCE
QUEEN ELIZABETH II CONFERENCE CENTRE, LONDON
27 JUNE-1 JULY 1994

**BY MEMBERS OF THE ISIS FACILITY**

**Papers to be published in the Proceedings of EPAC 94.**

August 1994

***Rutherford Appleton Laboratory*** Chilton DIDCOT Oxfordshire OX11 0QX

**CONTRIBUTIONS TO**

# EPAC 94

# LONDON

4th EUROPEAN PARTICLE ACCELERATOR CONFERENCE
EUROPHYSICS CONFERENCE
QUEEN ELIZABETH II CONFERENCE CENTRE, LONDON
27 JUNE-1 JULY 1994

## BY MEMBERS OF THE ISIS FACILITY

T W Aitken*, G M Allen, J R J Bennett, A I Borden, R A Burridge, T A Broome, M A Clarke-Gayther, C J Densham, P Drumm†, G H Eaton, W R Evans, I S K Gardner, M Glover, M Holding, J Kay*, G Martin, S Metcalf*, W Morris, G R Murdoch, H Price*, H Ravn†, G H Rees, T G Walker*, D D Warner* and C M Warsnop.

* DRAL staff (not from ISIS)
† CERN staff

**Papers to be published in the Proceedings of EPAC 94.**

August 1994

# CONTENTS

# ISIS Status Report

Ian S K Gardner
Rutherford Appleton Laboratory
Chilton, Didcot , Oxon, England.

*Abstract*

The recent accelerator development programme leading to increased operational intensity and to improved reliability of the ISIS pulsed neutron source is outlined. The methods used to control, minimise and measure beam loss are described. Some data on induced activity levels are given. The competing effects for accelerator component protection and spallation target survival are discussed.

## 1. INTRODUCTION

### *1.1 Facility Description*

The ISIS facility is based on a 70 MeV linac, an 800 MeV rapid cycling proton synchrotron and a spallation neutron target. The synchrotron was designed as a high current, low loss accelerator with $H^-$ charge exchange injection. The main use of the proton beam is for pulsed neutron production from the spallation target. The incident beam power on the spallation target is 160 kW, delivered as two 100 ns pulses separated by 200 ns at a repetition rate of 50 Hz. The maximum, operational, mean beam current delivered to date is just over 200 μA, and this corresponds to a circulating ring current of 6.2 A dc.

### 1.2 *Uses*

The facility is also a powerful source of pulsed muons and neutrinos and in addition supplies a beam of scattered particles from a vibrating internal target for testing particle detectors for the high energy physics instrumentation development at RAL. Irradiation experiments are carried out using both the 70 MeV $H^-$ linac beam and also the neutrons produced from the beam collectors in the synchrotron which are used to collect any beam which is lost during the trapping and acceleration processes.

### 1.3 *Operational Statistics*

The facility operates from 3500 to 4500 hours per year in 6 week cycles. User runs occupy 4 weeks of the cycle with the remaining 2 weeks being shared by maintenance, machine development and start up. Over 500 neutron scattering experiments were completed in 1993 and the ISIS neutron user community, which is international, is greater than 2000. Some operating statistics are shown in Table 1.

## 2. NEUTRON INSTRUMENT STATUS

The ISIS neutron instrument suite now numbers 15 and occupies 14 of the 18 available beam holes in the target shielding. The layout of the accelerator and instrument hall is shown in Fig. 1. As can be seen from the user statistics the average neutron experiment takes about 100 hours and scheduling of the large number of experiments requires a highly reliable accelerator, target station and set of neutron instruments, complete with a supply of sample environment equipment, such as cryostats, furnaces, pressure cells and magnets.The experiment programme covers the study of the structure, and the dynamic behaviour, of solids and liquids and includes most of the branches of science.

| | 1987 | 1988 | 1989 | 1990 | 1991 | 1992 | 1993 |
|---|---|---|---|---|---|---|---|
| | | | | | | | |
| Scheduled user time (days) | 176 | 182 | 178 | 167 | 175 | 145 | 149 |
| Beam time on target (days) | 128 | 132 | 131 | 131 | 135 | 122 | 126 |
| Beam time on target (%) | 73 | 72 | 73 | 78 | 77 | 84 | 85 |
| Integrated current mAhrs | 120 | 230 | 288 | 302 | 366 | 419 | 510 |
| $I_{pk}$, 24 hr average (μA) | 70 | 97 | 107 | 101 | 145 | 174 | 187 |
| μAhrs per beam trip | 6 | 18 | 31 | 61 | 44 | 63 | 75 |
| Targets used | U1,U2 | U3,T1 | U4,T1 | T1,U5 | U5,U6,T1 | T1,U7 | T1 |
| Neutron instruments | 7 | 7 | 10 | 12 | 13 | 13 | 14 |
| Neutron experiment reports | 168 | 174 | 253 | 330 | 343 | 428 | ~500 |

Table 1. ISIS operating statistics. U=Uranium target, T=Tantalum target.

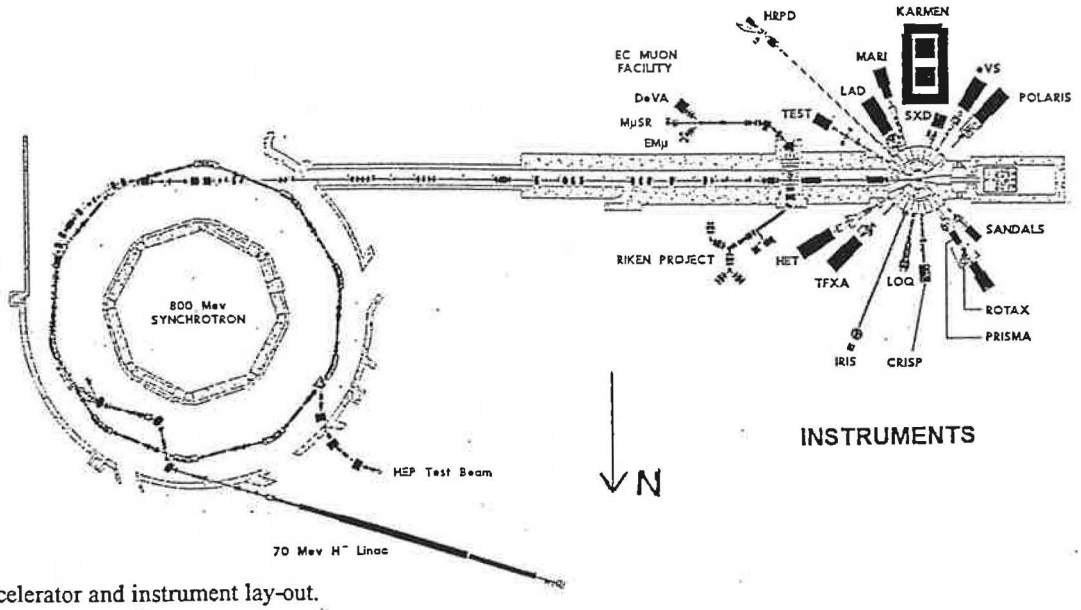


Fig. 1 ISIS accelerator and instrument lay-out.

## 3. MUON FACILITY STATUS

Muon beams are produced from a thin, water cooled transmission target made from graphite. Various thicknesses from 2.5 mm to 10 mm are used and the beam spot size at the target, which is 20 m upstream of the main neutron target, is about 20 mm diameter. The target provides surface or cloud muons for the EC Muon Facility on the South side of the experimental hall and pions for the decay muon channel on the North side. The EC-sponsored expansion of the original beam line was completed in June 1993, and allowed a 3-way split of the existing channel. Two $\mu^+$SR instruments for condensed matter research are operational.

The muon project on the North side is funded by the Japanese Science and Technology Agency through RIKEN. This consists of a superconducting solenoid and a pulsed magnetic kicker magnet to distribute muons with momenta up to 55 MeV/c to 3 experiment ports. The first muons are expected in October 1994 and the scientific programme will include: μCatalised Fusion, $\mu^{\pm}$SR and muonium spectroscopy.

## 4. TARGET SUMMARY

Target Station development has continued in parallel with the accelerator development and the performance of the Uranium targets and the one Tanatalum target is summarised in Table 2. The Tantalum target is still operational but there are some measurable changes in its cooling characteristics. It will be replaced in the summer of 1994.

The Uranium targets have failed at the lifetimes indicated in Table 2. It is thought that thermal cycling due to beam trips may effect their lifetime and there is a compromise between minimising the number of gross thermal cycles on the target and turning the accelerator off in order to protect the accelerator components from irradiation due to lost beam. A new Uranium target has been developed with a much smaller grain size than the earlier ones, and it is anticipated that this will give improved performance due to the slower and more random radiation growth in the Zircalloy clad Uranium target plates. This will be installed in the Autumn of 1994.

| | Gross Thermal Cycles | Integrated Current mAh | Neutron Production mg |
|---|---|---|---|
| U#1 | Not measured | 92.4 | 75 |
| U#2 | 40000 | 53.1 | 52 |
| U#3 | 10389 | 174.9 | 163 |
| U#4 | 4147 | 138.8 | 128 |
| U#5 | 5074 | 295.6 | 273 |
| U#6 | 2628 | 126.1 | 116 |
| U#7 | 1805 | 107.2 | 99 |
| Ta#1 | 70746 | 1638.9 | 970 |

Table 2. Neutron target operating data. U=Uranium, T=Tantalum

## 5. ACCELERATOR SUMMARY

*5.1 Recent Development Programme*

In 1989, an improvement programme was started on the accelerators and beam lines following the signing of a joint funding agreement between the German BMFT and the UK SERC. This was aimed at increasing the operating intensity of the accelerators to the original design value of 200 μA and to increasing the beam availability to 90%. This specification was required for the neutrino experiment KARMEN to achieve good measurement statistics.

The first improvement was the replacement of the 3 pulsed ferrite extraction kicker magnets. The original magnets had been damaged by beam loss and voltage breakdown. The new magnets are designed for higher voltage and ease of maintenance when active. Since installation, they have required very little maintenance and the synchrotron energy has been increased from 750 to 800 MeV.

The number of programmable dipole correction magnets was increased from 4 to 6 for the horizontal plane and from 4 to 7 for the vertical plane. These allow the measured closed orbit distortion to be less than 3 mm rms throughout the acceleration cycle. In setting up the synchrotron, the orbit distortion is first minimised and then further small adjustments are made to ensure that the untrapped beam is all picked up on the six beam collectors situated in super periods 1 and 2. Figure 2 and 3 show a plot of the beam intensity and the beam loss [1] during the acceleration cycle.

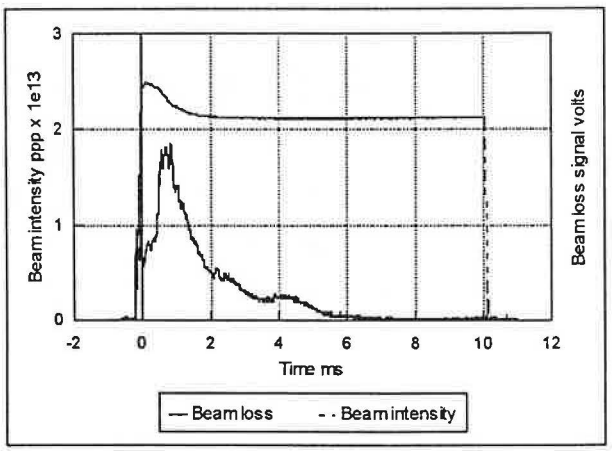


Fig. 2. Beam intensity and beam loss monitors sum signal during acceleration.

Although the original synchrotron design envisaged that the Q-values would only be altered during the multi-turn beam injection period, with minor adjustments for the rest of the cycle, it has been found beneficial to programme the Q-values throughout the full cycle. In addition $7^{th}$ and $8^{th}$ harmonic modulations of the 20 programmable quadrupoles

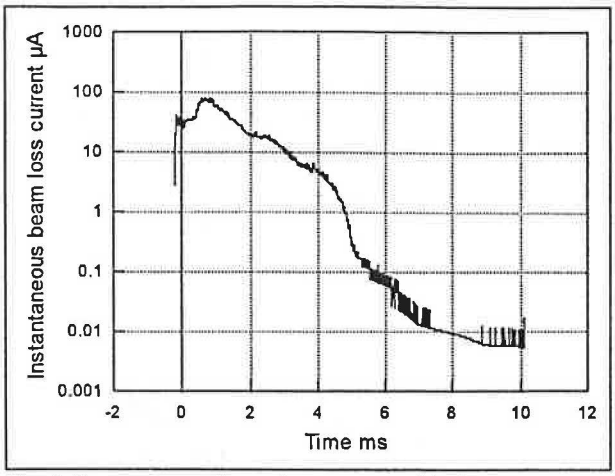


Fig. 3. Instantaneous beam loss current with time.

are used to minimise the beam loss during acceleration. The Q-value variation with time is shown in Figure 3 along with the calculated Q-values allowing for the maximum incoherent tune shift due to space charge. As can be seen the $Q_h$=4.0 resonance is crossed by some particles very soon after trapping. Small deviations from the Q-value locus shown result in large beam loss, as do increased closed orbit errors; the increase in betatron motion due to crossing the integer resonance for a closed orbit error has been estimated [2].

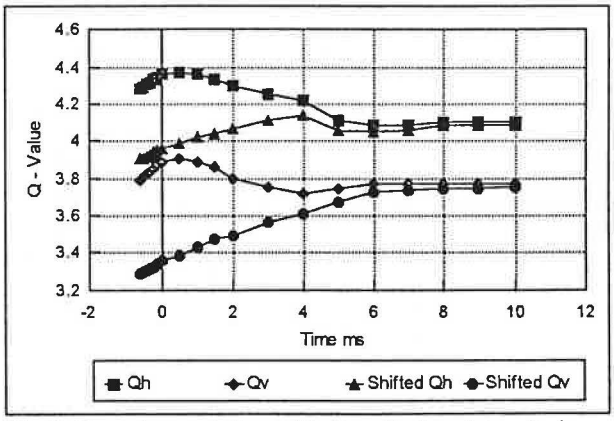


Fig 4. Q - value variation with time for low intensity beam and maximum incoherent tune shift due to space charge.

Two further factors dominate the maximum achievable beam intensity and these are the distribution of the horizontal and vertical betatron amplitudes of the beam during injection and the momentum distribution of the injected beam. A beam diagnostic system for measuring these parameters has now been completed to an initial stage. It makes use of a beam chopper in the 70 MeV $H^-$ linac to ring beam transport line [3]. This selects a beam pulse of a fraction of a turn (200 ns) at any time in the injector pulse . Use is made of position monitors and a digital storage oscilloscope to track the beam

pulse on many turns. The betatron amplitudes in each plane can be measured along with many other parameters of the synchrotron. In addition by measuring the rate at which the beam debunches then the momentum spread can be deconvoluted. Typical outputs from the system are shown in Fig 5, 6 and 7. The required variation of vertical betatron amplitude is produced by a programmable magnet in the 70 MeV beam transport line.

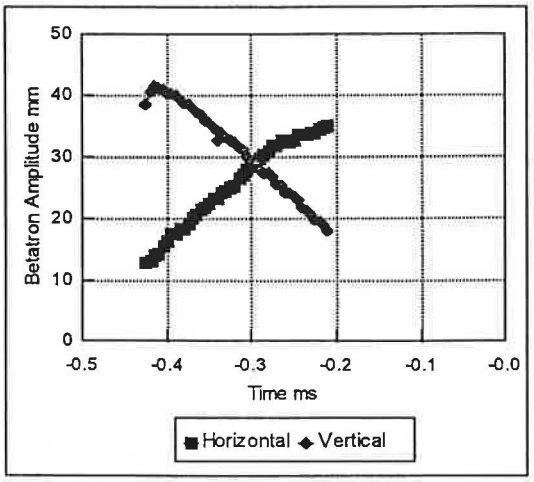


Fig. 5. Horizontal and Vertical betatron amplitudes during injection.

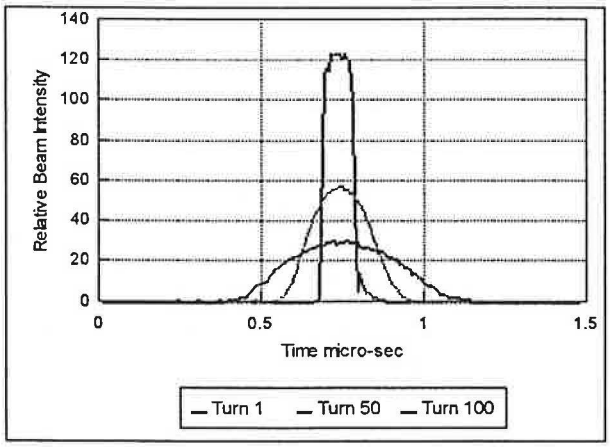


Fig. 6. Chopped beam pulse debunching over 100 turns.

The 6 RF accelerating systems in the synchrotron continue to work well following the change to the double 500 kW valve configuration. The feed forward beam loading compensation system [4] requires only occasional adjustment and copes easily with beam intensities of 2.5 $10^{13}$ ppp. Beam phase and radial control loops are used to maintain stable operation.

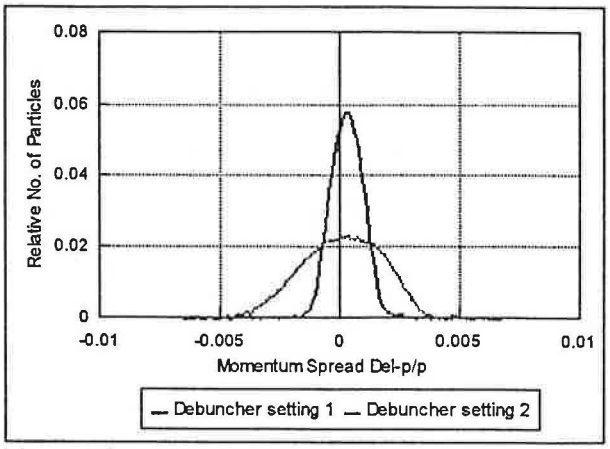


Fig. 7. Injected beam momentum spread for two different debuncher settings.

*5.2 Induced Activity Levels and Beam Collection*

The induced activity levels on the synchrotron and 800 MeV transport line have remained at the same level for some years now as the allowed rate of beam loss has been maintained at the same level although the operating beam intensity has increased. The sum of the radiation levels from 12 fixed monitor points on the synchrotron survey pillars, subsequent to beam turn off, are shown in Table 3. The beam loss protection system will turn the beam off following beam loss in one of five possible modes. These modes operate in different time periods with the shortest being 60 ms and the longest 500 ms. The system also detects the loss of beam other than on a beam collector, and if this is above a pre-set level this will initiate a beam trip.

| Day 2 Radiation level μSv/hr | Day 20 Radiation level μSv/hr | Day 40 Radiation level μSv/hr | Day 60 Radiation level μSv/hr |
|---|---|---|---|
| 353 | 194 | 150 | 116 |

Table 3. The sum of the radiation levels at the mechanical survey pillars following synchrotron shut-down.

## 6. NEW DEVELOPMENTS

*6.1 Potential Developments*

There are several potential developments of the ISIS accelerator and target that could enhance the facility and make it available to a larger number of concurrent users than at present. Such developments include a second target station operating at a repitition rate of about 10 Hz, and a

radioactive ion beam source 10 or 100 times more powerful than any presently in existence. However, to introduce these facilities without reducing the performance of the present neutron, muon and neutrino fluxes, requires the intensity of ISIS to be increased.

Recent theoretical studies of the synchrotron [5] have shown that the addition of a second RF system working at twice the frequency would increase the intensity from 200 to 300 μA. Implementation of this system would require an increase in the linac current and this may be possible following the development of an RFQ pre-injector. Operation at 300 μA with 200 μA being delivered to the present target station as 2 out of every 3 beam pulses allows two 50 μA proton beams at 8.33 Hz for additional facilities such as a second target station and a radioactive ion beam facility.

### *6.2. RFQ Development*

The RFQ development comprises an $H^-$ ion source injecting into a Radio Frequency Quadrupole linear accelerator and is being designed to replace the present 665 keV High Voltage DC Accelerator, Low Energy Beam Transport and Bunching system. The present high voltage power supply is very old and it is becoming increasingly difficult to obtain spares for the system. The system also suffers from spark downs that discharge the accelerating column. The effects of these on integrated current have been reduced, but the basic problem remains. The high space charge forces, beam loading and the optical aberrations within the column also produce a deterioration in beam quality. The ion source, which fits inside the input end of the column, is not easily accessible.

The RFQ is designed to both bunch the beam and accelerate it to 665 keV at a transmission efficiency of greater than 90% (c.f. 60% with the present system). It should also be possible to obtain better optical matching and alignment into the Drift-Tube linac(DTL). The accelerating voltage for injection into the RFQ is only 35 keV and it will allow ion sources to be changed more quickly. The RF power drive for the RFQ will be identical to part of the existing amplifier chain powering the accelerating cavities of the DTL. Such a pre-injector system should remove the high voltage breakdown problem and improve the transmission efficiency and beam quality into the downstream accelerators.

### *6.3. Radioactive Ion Beam Source Development*

The aim of this programme is to build a test bed facility for use on ISIS, to develop the technology to generate radioactive nuclei in a suitable target using a 100 μA, 800 MeV proton beam, and to produce ionised beams of selected species. The programme is part of a European and world-wide effort to produce a proposal for a radioactive ion beam accelerator. The test bed is being built off line and will be installed in the ISIS target station in 1996 for tests with the proton beam.

## 7. AKNOWLEDGEMENTS

This paper summarises some of the work of the staff of the ISIS facility.

## 8. REFERENCES

[1] M.A. Clarke-Gayther, A.I. Borden and G.M.Allen,Global Beam Loss Monitoring Using Long Ionisation Chambers at ISIS.Proceedings of this conference.

[2] G.H. Rees and C.R. Prior, Image Effects On Crossing An Integer Resonance. Submitted to Particle Accelerators 1994.

[3] C.M. Warsop, Low Intensity and Injection Studies on the ISIS Synchrotron. Proceedingof this conference.

[4] P Barratt, I Gardner, C Planner and G Rees, RF System and Beam Loading Compensation on the ISIS Synchrotron. Proceedings of the Second European Particle Accelerator Conference, Nice, France, 1990, p949-951.

[5] C.R. Prior, Study of Dual Harmonic Acceleration in ISIS. Proceedings of the Twelfth Meeting of the International Collaboration on Advanced Neutron Sources.Abingdon, UK, 1993.

# Important Design Issues of High Output Current Proton Rings

G. H. Rees
Rutherford Appleton Laboratory
Chilton, Didcot, UK.

*Abstract*

High output currents of protons are required for future pulsed spallation neutron sources and Kaon Factories. Typical parameters are 5 mA at 1 GeV or 1.667 mA at 3 GeV for the former, and 0.1 mA at 30 GeV for the latter. The resulting beam powers are 5 and 3 MW, respectively, so that key issues are low beam loss and reliable beam loss protection. The following aspects of the rings' design are considered here: very high efficiency $H^-$ injection, beam optical parameters, vacuum enclosures, radio frequency containment and acceleration, instability considerations, magnet systems, low loss extraction, beam loss collimation and collection, and shielding.

## 1 INTRODUCTION

Large extrapolations of output proton currents have been proposed for rings of future pulsed spallation neutron sources and Kaon Factories. Both types of facility propose a high repetition frequency ($\lesssim$ 50 Hz): in addition, neutron sources consider enhanced values of circulating currents. Typical output parameters are 5 mA at 1 GeV, 50 Hz, or 1.667 mA at 3 GeV, 50 Hz for the former, and 0.1 mA at 30 GeV, 10 Hz for the latter.

There are a number of accelerator options for the spallation sources: linac and accumulator rings, linac and fast cycling synchrotrons, linac and FFAG accelerator(s), a Kaon Factory type facility or an induction linac. Of these, the first two are currently favoured, and for each it appears advantageous to use more than one ring. Kaon Factories have been studied over many years, both in North America (the TRIUMF KAON and Los Alamos AHF studies) and in Europe (the EHF and the studies at INR, Troisk). Common to these designs is the use of a booster and main ring synchrotron, supplemented by one or more of the following: accumulator, collector, extender. Despite all the studies, no Kaon Factory has received a final approval.

The many rings of the Kaon Factories present a wide range of machine physics issues, far more than do the rings of the proposed spallation sources. However, though the issues are fewer for the latter, they are more challenging because of the higher peak circulating current in the rings.

Kaon Factory studies have been reported extensively, and it is sufficient for this paper to list the relevant design issues, quoting appropriate references. The paper then concentrates on new design issues for the next generation, 5 MW, pulsed spallation sources. A key issue is the design for ultra low loss $H^-$ charge exchange injection.

## 2 RING DESIGN ISSUES

Kaon Factory designs have had to consider the overall reliability and availability of a facility that has a number of complex, high power rings (3,4 or 5) feeding each other in sequence, so that a failure of any one ring or of the injector leads directly to experimental down time. Individual issues of importance are given in the form of a list:

$H^-$ painting ($H^0$ states),[1]
Beam loss collection,[2]
Betatron resonances,[3]
Heavy beam loading,[4]
Electron-proton instability,[5]
Fast extraction,[6]
Ceramic vacuum chambers,[7]
High transition energy lattices,[8]
Synchrobetatron resonances,[9]
Polarisation (Siberian Snakes),[10]
Low loss slow extraction,[11]
Coupled bunch instabilities,[12]
Longitudinal emittance enhancement.[13]

By comparison, the favoured schemes proposed for a 5 MW spallation source consist of a high energy linac and either 2 accumulator rings operating in parallel, or 2 rapid cycling synchrotrons providing output beams in alternate cycles. Then, the loss of a single ring leads only to a halving of intensity, an important consideration due to the short turn around time of neutron scattering experiments.

The first seven items on the Kaon Factory list also apply to the spallation sources, where the larger circulating currents give them more significance. One consequence is that the spallation sources require ultra low loss $H^-$ injection, which, in turn, calls for a new form of halo containment for the $H^-$ linac beam.

Radiofrequency systems for the spallation source rings are different from those for the Kaon Factories. The rapid cycling, large radius main ring of the latter requires a large voltage gain per turn. A frequency of approximately 50 MHz is used to provide this voltage, and also to allow short bunch kaon experiments, in a fast extraction mode.

Lower frequency, dual harmonic systems are selected for the spallation sources, where the ring radii are smaller, with h=1 and 2 in the accumulators, and h=2 and 4 in the rapid cycling synchrotrons. The systems allow improved momentum painting during injection, and lead to lower beam bunching factors and transverse space charge forces. A further gain occurs as the natural bunch gap is sufficient for the risetime of a fast extraction kicker magnet. Total proton pulse durations have to be $<1$ $\mu$s.

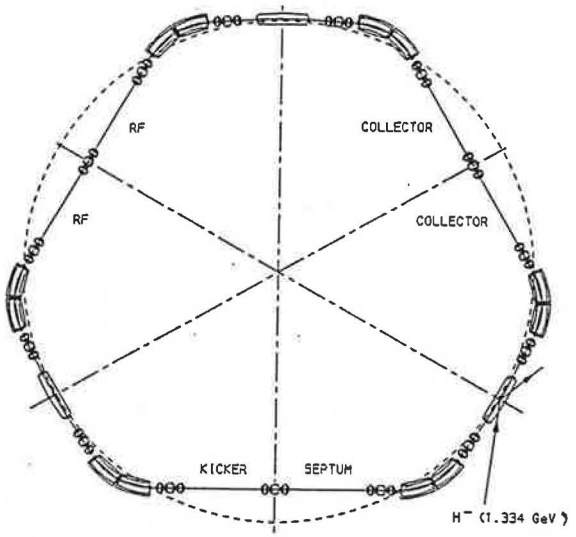


Figure 1. 1.334 GeV Accumulator

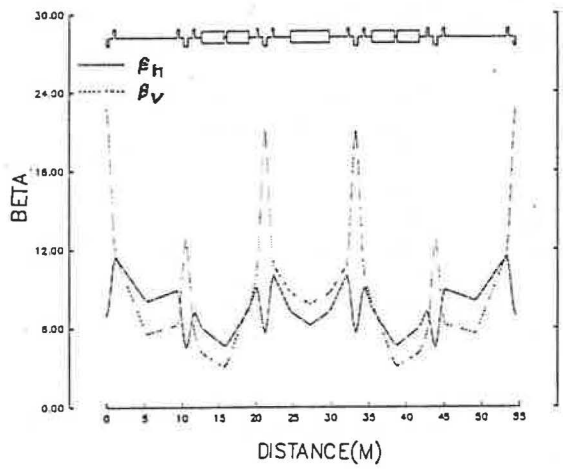


Figure 2. Accumulator β-Functions

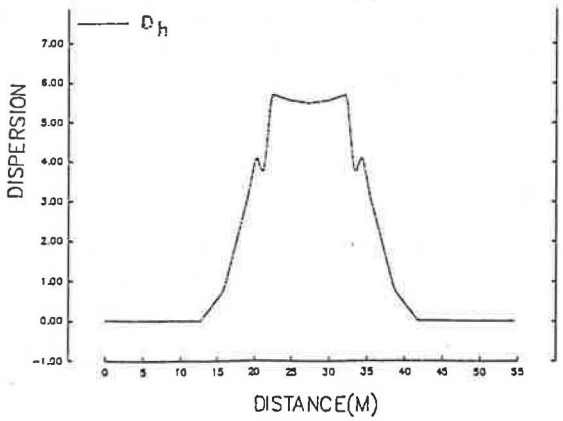


Figure 3. Accumulator Dispersion

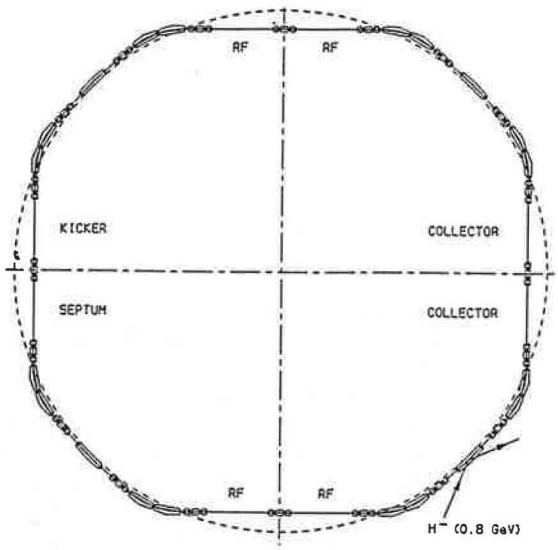


Figure 4. 3 GeV Synchrotron

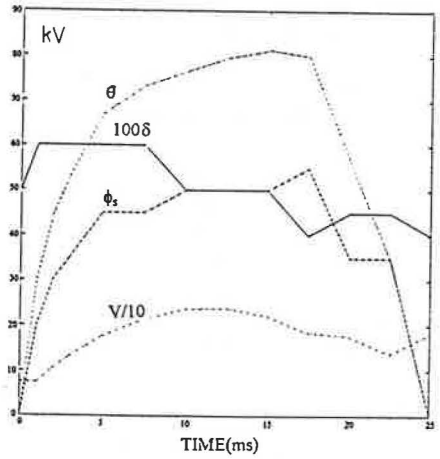


Figure 5. Synchrotron RF Parameters

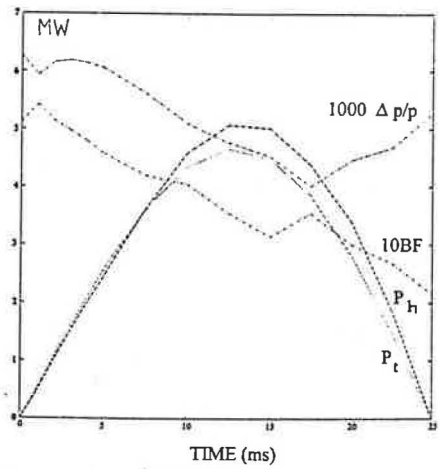


Figure 6. RCS Beam Power and Δp/p

An overview of future spallation neutron source designs is given in [14], including some linac and target considerations, not considered here. Important issues for the spallation source rings are now addressed separately.

## 3 $H^-$ INJECTION

Developments in $H^-$ injection systems are described in [1], and the system proposed for a possible 5 MW pulsed source, the European ESS facility, is shown in Figures 7 to 11. Magnet lattices are designed around the injection region; Figure 1 is for a pair of 1.334 GeV accumulators and Figure 4 for a pair of 3 GeV rapid cycling synchrotrons (RCS), both of which are options for the ESS.

At the centre of the injection region is a low field lattice dipole, of a length and bend angle that allows a direct ring exit for unwanted $H^0$ and $H^-$ particles emerging from the stripping foil. Most of the incoming beam strips to protons within the ring acceptance and continues to circulate, merging with the incoming $H^-$ beam in the centre of the low field dipole. The choice of the field in this dipole is important. It is chosen to give negligible prestripping of $H^-$ ions ahead of the foil, to minimize delayed stripping of $H^0$ atoms within the ring and to provide a bending radius for the stripped electrons large enough for direct collection, see Figure 10. Different fields are chosen for some ESS options: 0.177 T for the 1.334 GeV accumulators, 0.1252 T for the 0.8 to 3.0 GeV RCS, and 0.1252 T for a 3 ring, 0.8 GeV accumulator option. Identical lattices may then be chosen for the 1.334 and 0.8 GeV accumulators.

A foil thickness is chosen which strips ~98.5% of the $H^-$ beam to protons (eg 345 $\mu$gm $cm^{-2}$ $Al_2O_3$ for 1.334 GeV $H^-$), leaving most of the rest as partially stripped $H^0$ atoms, in a range of quantum states. The fate of these depends on their Stark state in the injection magnet. Energy levels for states of principal quantum number n=4,5 and 6 are given as a function of electric field in Figure 8; the vertical dashed lines are the E field equivalents for the B fields of the different options (eg option 2 is for the 1.334 GeV accumulators). Atoms of low n value (<4) remain as $H^0$ and pass out of the ring for collection; atoms of high n (>6) strip rapidly and are accepted as protons; there remain some intermediate states which strip after some delay, so may be accepted or lost, or become beam halo. The atomic physics is discussed in [15], and a semi-empirical formula derived for the Stark state lifetimes. Those for the states n=4 and 5 are plotted in Figure 9 for the 1.334 GeV $H^0$ atoms. There is a gap in the graph between the n=4 and n=5 states, and the chosen field of 0.177 T is within this gap. Direct transitions between the two states bordering the gap and the stripped state are forbidden, so the effective gap is enhanced. The options 1 and 3 have injection at 0.8 GeV, and the field of 0.1252 T then corresponds to an equivalent gap between the states n=5 and 6.

It is proposed to use a foil with two free, unsupported edges to reduce the subsequent proton foil traversals. Simultaneous painting is provided in the longitudinal and both transverse planes. Vertical painting is obtained by collapsing the field in the 4 vertical bump magnets, shown in Figure 7. Correlated horizontal and longitudinal painting results from the choice of a finite dispersion at the foil together with a ramping of input beam momentum. The longitudinal painting is improved by chopping the linac beam with a 60% duty cycle at the ring bunch repetition frequency, and also by amplitude and frequency modulation of the dual radiofrequency systems. The transverse painting commences with large horizontal and small vertical oscillations and changes gradually to end with the reverse correlations. Foil traversals are also reduced by mismatching the linac and ring beams, with zero dispersion and low beta parameters for the former at the foil.

Beam losses may result from delayed stripping of $H^0$, or from inelastic and elastic foil interactions; betatron and momentum tails form, adding to those due to linac beam halo. A negative momentum tail and dispersion at the foil increases the losses. Overall losses are acceptable, however, since there are few foil traversals for the proposed 1000 turn painting. A proviso is that incoming beam halos, longitudinal included, must be at acceptable levels, and this is a new area for linac studies.

Other schemes employ zero dispersion at the foil, merging the $H^-$ beam and protons either in a lattice dipole or in a dipole of a bump magnet set. For these, orbit bumps create less favourable final distributions, with rectangular beam cross sections.

The vertical bump magnets are all within the injection cell, thus separating the ring and injection optics. The price to pay for this layout is a high power current supply, which must be collapsed over the 600 $\mu$s injection interval. The peak power is >10 MVA for the ESS design, and varies inversely as the cube of the length, l, see Figure 7.

## 4 RING PARAMETERS, VACUUM

Large transverse emittances are required to restrict the space charge tune shifts and the proton foil traversals. The chosen 1 $\sigma$ phase space areas ($/\pi$) are 30 and 35 $\mu$rad m for the 1.334 GeV ESS accumulators and 0.8 GeV-injection ESS options, respectively. Machine acceptances (4 $\sigma$) are 480 and 560 $\mu$rad m, respectively, and collimator limits are set at 260 and 305 $\mu$rad m.

Longitudinal bunch areas are chosen to avoid potential instabilities. Each ESS accumulator has a bunch area of 6.5 eV sec, while each ESS RCS has 2 bunches with 5 eV sec per bunch. These values are based on the use of contoured vacuum chambers to reduce the longitudinal space charge forces. For the chosen transverse and longitudinal emittances, the required values of normalised lattice dispersion at the position of the foil are ~2.2 $m^{1/2}$.

It is planned to shape the vacuum vessel dimensions to be a constant ratio of $4/\sqrt{5}$ to the local values of the full beam sizes in the rings. Solid chambers of aluminium are assumed for the accumulators, but ceramic chambers are needed for the RCS main and correction magnets. The ceramic chambers may follow the ISIS designs of [7], and require ISIS-style contoured radio frequency inter-shields.

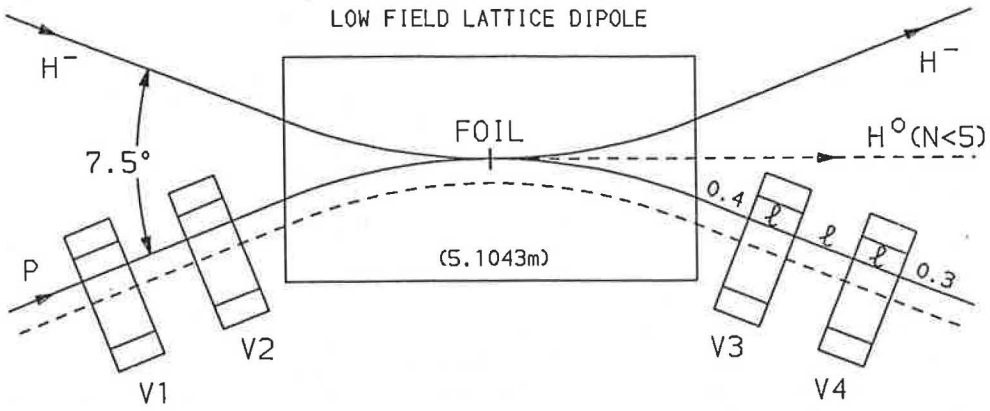


Figure 7. $H^-$ Injection Straight Section

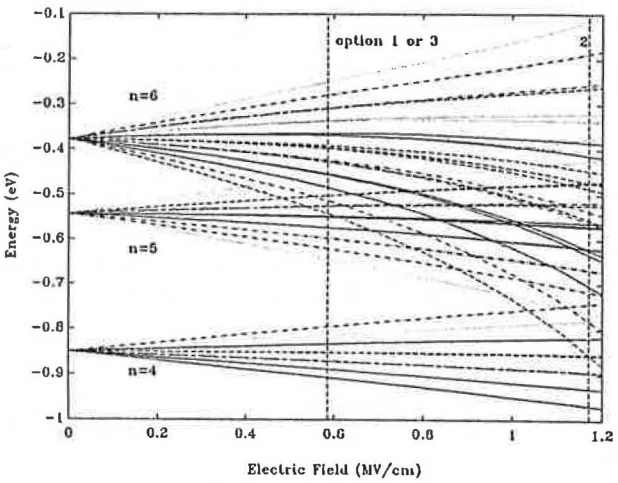


Figure 8. Energy Levels of Stark States

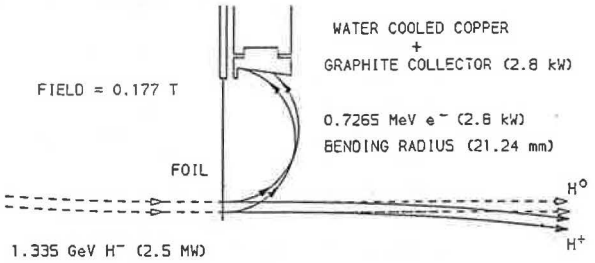


Figure 10. Electron Collection on Stripping

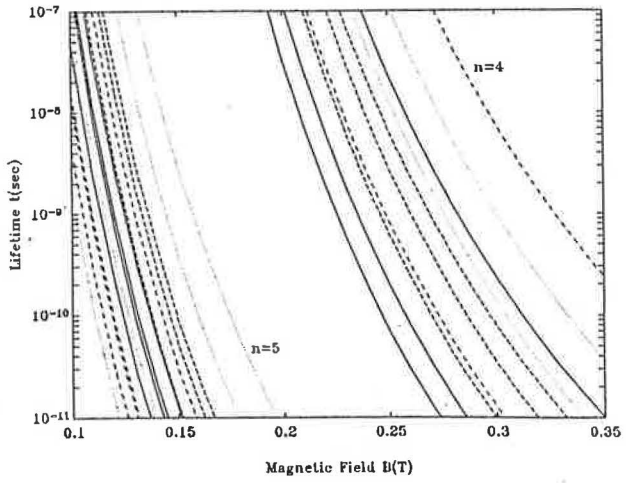


Figure 9. Stark State Lifetimes in Lab Frame

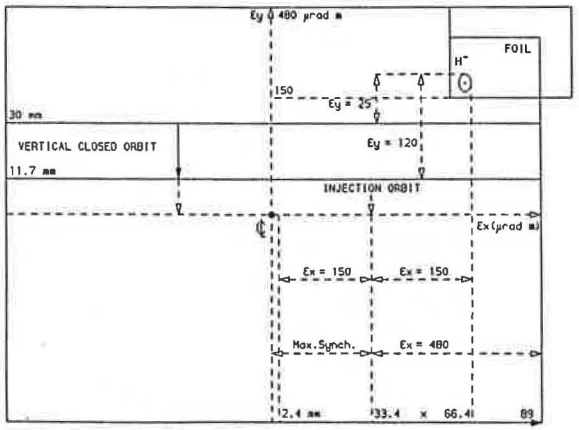


Figure 11. Cross Section at Stripping Foil

## 5 RADIO FREQUENCY SYSTEMS

Dual harmonic systems are proposed with total voltages:
$V = V_0$ (sin h$\omega$t - $\delta$ sin(2h$\omega$t + $\theta$))
(though Barrier Bucket systems are also to be studied). For the accumulators, h=1, $\theta$=0, $\delta$=0.5, $V_0$ is raised from ~8 to 30 kV over injection and $\omega$ is frequency modulated. For the RCS, h=2, and $\theta$, $\delta$, $V_0$ and $\omega$ change continuously, see Figures 5 and 6. All options have heavy beam loading, reactive in the accumulators, but reaching 5 MW peak resistive in each RCS at mid-cycle. $P_t$ and $P_h$ of Figure 6 are, respectively, the total beam power and that provided by the system of harmonic, h. When $P_t$<$P_h$, power is absorbed from the beam by the 2h cavity systems. Longitudinal tracking is used to check parameters. Cavities have a single gap for the accumulators, but two gaps for the 25 Hz RCS, where 240 kV peak per turn is required.

## 6 INSTABILITIES

Bunched beam instabilities alone are relevant as the $H^-$ beam is chopped at the ring bunch repetition frequency and cavities are on through injection to extraction. Though bunched, the beam may still develop an electron-proton instability, as at the PSR, LANL. It is suspected, but not confirmed, that their 30 $\mu$s growth time instability is caused by protons migrating into the bunch gap and attracting electrons, formed at pinger and extraction plates, in some avalanche process. The instability does not occur in ISIS at 70 MeV for equivalent levels (4 $10^{13}$ protons), not even in a coasting beam mode. The ESS flux is ~6 larger, but this is offset by larger bunch areas and higher energies. ISIS safeguards are to be adopted: smooth chamber transitions, collection of foil stripped electrons and the use of low impedance, ferrite extraction kickers. Accumulators are potentially safer than RCS as beam is in them for less time, they have fewer cavities and they use solid vacuum chambers, not ceramic with inter-shields. Use of natural chromaticities leads to large head-tail phase shifts, reducing the prospect of transverse instabilities.

## 7 MAGNETS AND EXTRACTION

ESS dipole field levels, except in the injection dipoles, are 1.13 T in the 1.334 GeV accumulators, and 0.42 to 1.1 T in the RCS. They are dc in the accumulators and have a 20 Hz sinusoidal rise, a 40 Hz fall, and a 2.5 ms flat bottom in the RCS. Quadrupole and bending magnets have apertures comparable to those used in the ISIS ring.

Kicker risetimes must be <190 ns for the accumulators and <300 ns for the RCS. Push-pull, lumped kickers, separated by a ground plane, are to be used, as at ISIS. One design has a pulse forming network ($Z_0$/2), speed-up network and thyratron feeding a resistor $Z_0$ in parallel with a $Z_0$ cable linking a half kicker, again as at ISIS. Another has a PFN at $Z_0$, thyratron, and $Z_0$ cable feeding a saturating inductor and half kicker, with a speed-up network in parallel. Voltages and kicker currents are 40 kV and 5 kA, respectively, though the thyratron currents for the latter are halved. Coupling impedances for the designs will be checked. Required are 3x2 for the 0.8 GeV rings, 4x2 for the 1.334 GeV rings and 4x2 for the RCS. Lumped kickers are preferred to less rugged delay-line types.

## 8 COLLIMATORS AND SHIELDING

Beam loss may be localised by collimators and collectors. These are in a dispersion free region for betatron collection and at a point of maximum normalised dispersion for momentum loss. The former are more important for the accumulators, the latter for the RCS. For betatron loss, the primary collimators are set at a normalised transverse position, Z, and the secondary collectors at $Z_1$ and -$Z_1$, after betatron phase shifts $\mu_1$ and $\mu_2$, respectively. Requirements are $Z_1 > Z$ and $Z_1 \cos \mu_1 = Z = -Z_1 \cos \mu_2$. Typical values are $\mu_1$=15°, $\mu_2$=165°. It helps to angle the upper or lower half of the collimators, and to have $\mu_2$ equal in the two transverse planes over the region. Collectors have to stop primary particles; the first is set just downstream of a collimator, with its surface set back progressively as the distance downstream increases, with $Z_1$(max) typically 1.02 Z. Large tunnels are envisaged for the rings, ~10 m by 15 m to allow hands on maintenance. Shielding will be 1.5 m steel, covered by 1.5 m of concrete, both for rings and beam lines to the neutron targets.

## 9 REFERENCES


[1] G.H.Rees, "Injection", Proceedings of General Course of CERN Accelerator School, CERN 94-01, 1994, p.737
[2] H.Schönauer, "Predeflectors for Beam Loss Concentration", Proceedings of EPAC 92, Berlin, 1992, p.339
[3] G.Guignard, "Selection of Formulae Concerning Proton Storage Rings" Section 10, CERN 77-10, 1977, p.66
[4] D.Boussard, "Beam Loading", Proc. of CERN Accelerator School, CERN 87-03, 1987, p.626
[5] T.Wang et al, "Recent Study of Beam Stability in the PSR", Proc. of IEEE PAC, Washington, 1993, p.3297
[6] M.J.Barnes et al, "Improving Kicker Systems", Proc. $XV^{th}$ Int. Conf. on H. En. Acc, Hamburg, 1992, p.191
[7] J.R.J.Bennett et al, "Glass Jointed Alumina Vacuum Chambers", Proc. IEEE PAC,Washington, 1981, p.3336
[8] R.V.Servranckx, "Racetrack Lattices for the TRIUMF Kaon Factory", Proc. IEEE PAC, Chicago, 1989, p.1355
[9] R.Baartmen et al, "Synchrobetatron Resonances", Proc. of EPAC 90, Nice, 1990, p.1627
[10] "The TRIUMF Kaon Factory Project Definition Study", 2.1.5 Polarized Beam, May 1990, p.2-19
[11] U.Wienands et al, "Slow Extraction for KAON with 0.1% Losses", Proc. EPAC 88, Rome, 1988, p.269
[12] "The TRIUMF Kaon Factory Project Definition Study", 5.1, Collective Instabilities, May 1990, p.5.1
[13] S.Koscielniak and G.H.Rees, "Longitudinal Emittance Blow-up", Proc. of EPAC 90, Nice, 1990, p.1741
[14] G.H.Rees "Overview of Future Spallation Neutron Sources", Proc. IEEE PAC, Washington, 1993, p.3731
[15] R.J.Damburg et al, Chap. 3, Rydberg States of Atoms and Molecules. F.Stubbings, Camb. Univ. Press, 1993

# The RIST Project at ISIS

J R J Bennett, R A Burridge, T A Broome, C J Densham, W R Evans, I S K Gardner, M Holding, G R Murdoch and T G Walker
DRAL, Rutherford Appleton Laboratory, Chilton, Didcot, Oxen, OX11 0QX, UK.
T W Aitken, J Kay, S Metcalf, H Price and D D Warner
DRAL, Daresbury Laboratory, Daresbury, Warrington, Cheshire, WA4 4AD, UK.
P Drumm and H Ravn
CERN, CH - 1211 Geneva 23, Switzerland.

*Abstract*

A description is given of the Radioactive Ion Source Test (RIST) Project to develop a target and ion source to produce intense beams of radioactive ions using the proton beam of the pulsed neutron scattering Facility, ISIS[1] at the Rutherford Appleton Laboratory. A tantalum foil target is bombarded by 800 MeV protons at currents of up to 100 μA. The target is kept at temperatures of 2000 - 2700 K. The radioactive particles diffusing out of the foils are ionised on a hot tungsten surface. The ions pass into a magnetic analyser and are identified by nuclear detection techniques.

## 1. INTRODUCTION

Radioactive nuclear beams have important, exciting and increasing uses in a wide area of science:-

- Nuclear Astrophysics
- Nuclear Physics
- Solid State and Atomic Physics
- Biology and Medicine

Radioactive nuclei can be produced by the impact of high energy protons on a thick target. This is the method employed by the on-line isotope separator, ISOLDE[2], using proton currents of up to 2 μA from the 1 GeV PS-Booster at CERN. The RIST Project is aimed at the development of a target and ion source to produce higher intensity radioactive beams. The world leading pulsed neutron facility, ISIS, with proton currents of up to 200 μA from the rapid cycling 800 MeV synchrotron, is well placed to carry out this development.

This project is part of a European and world-wide R&D programme to produce a proposal for an advanced radioactive ion beam accelerator facility.

## 2. THE AIMS

The aims of the project are specific and limited:-

a) To produce unstable nuclei from a tantalum target using the 800 MeV proton beam from ISIS, with mean proton currents of up to 100 μA.

b) To show that the radioactive ion currents are comparable to those of other similar sources, such as ISOLDE at CERN, at the same proton beam current on the target.

c) To show that the beams of these isotopes are increased in proportion to the proton current on the target.

d) To examine fluctuations of the high voltage on the target and ion source when the target is bombarded by intense pulsed proton beams.

## 3. THE TARGET AND ION SOURCE

The target and ion source will be built as closely as possible to the ISOLDE design so that comparisons of the performance are relevant. To limit the tests, only a tantalum target will be built. This will provide a wide range of radioactive particles, in particular the alkali metals and rare earths. The ISOLDE target consists of a tube containing short lengths of rolls of thin, 25 μm, tantalum foils. The tube is 2 cm in diameter and 20 cm long. The equivalent length of tantalum foil, through which the proton beam passes, is ~10 cm. The target absorbs about 600 W at 2 μA proton current.

The RIST target will be the same size as the ISOLDE target but will absorb up to 30 kW of proton beam power. To dissipate the higher beam powers in the RIST target it is necessary to change the configuration of the foils in the target tube. Good thermal conduction is required between the foils and the tube. To minimise the temperature rise in the foils they will be arranged effectively as a stack of discs welded to the inside of the tube. Each disc is 25 μm thick and spaced from its neighbour by 25 μm.

The target must be heated to temperatures of 2000 - 2700 K for sufficiently rapid diffusion of the short lived isotopes out of the thin foils. Electron beam heating will be used to heat the target at low proton beam currents. The particles then pass into an ion source. For simplicity a hot tungsten surface ioniser will be used similar to that employed at ISOLDE.

Dissipation of the heat from the high temperature target will be by thermal radiation to the surrounding water cooled vacuum vessel. The target must have no cold spots which could condense some of the products nor must it be allowed to become so hot that the target melts. Thermal stress must be minimised since tantalum is very weak at high temperatures. Thus the design must be optimised to keep the target at as uniform temperature as possible. A tapered hole through the centre of the target foil discs maintains the same beam power dissipation along the length of the target,

helping temperature uniformity. Tests of the thermal properties of the target are underway.

## 4. THE SEPARATOR

The RIST target will be inserted through the top plug of the target station shield to replace the ISIS neutron production target which will be moved back to act as a beam stop. The target and ion source is at 30 kV and the radioactive ions are accelerated to ground potential and focused by an Einzel lens through a 5 cm diameter hole in the shielding to the top of the target station. All subsequent focusing is by electrostatic quadrupoles. A number of Faraday cups and slits are strategically placed along the beam line for setting up and measuring the beam. On emerging from the top of the shield plug, the ions are bent into the horizontal plane by a 90° electrostatic deflector and pass through a 60° bending magnet for mass separation. Finally their intensity and identity will be determined by Faraday cup and nuclear detection techniques. Figure 1 shows an illustration of the RIST equipment in the target station and an inset view of the target.

## REFERENCES


[1] J L Finney, "ISIS: A Resource for Neutron Studies of Condensed Matter", Europhysics News, vol 20, 1989.

[2] H J Kluge (Editor), "ISOLDE Users Guide", CERN 86-05, 1986.

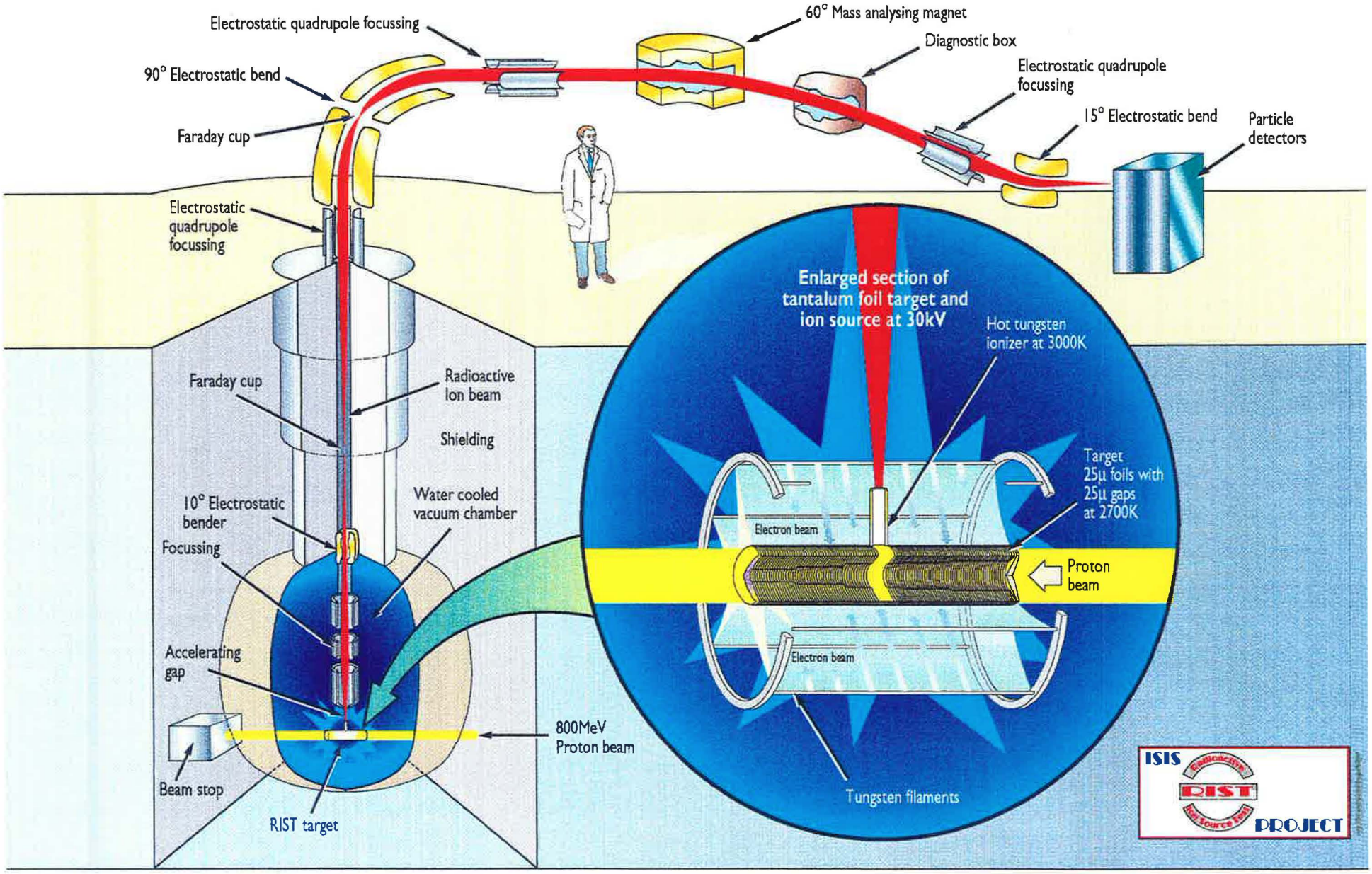


Figure 1 Illustration of the Radioactive Ion Source Test Project, RIST

# Global Beam Loss Monitoring Using Long Ionisation Chambers at ISIS.

M.A.Clarke-Gayther, A.I. Borden and G.M.Allen
Rutherford Appleton Laboratory
Chilton, Didcot, UK.

*Abstract*

A description is given of the global beam loss monitoring system at ISIS, the high intensity pulsed neutron source at the Rutherford Appleton Laboratory. The system has proved to be an important machine tuning and protection diagnostic, and has enabled a regime of 'hands-on' maintenance to continue, with operational mean proton currents in excess of 180 $\mu$A.

## 1 INTRODUCTION

ISIS is now the most intense pulsed neutron source for condensed matter materials research in the world. Operational from December 1984, the fast cycling (50 Hz) proton synchrotron is now running close to its design intensity (200$\mu$A), and routinely delivers mean proton currents in excess of 180 $\mu$A to a tantalum or depleted uranium target.

Calculations, performed during the machine design phase, indicated that operational beam loss would need to be carefully minimised, on a machine wide (global) basis, if the required regime of 'hands-on' maintenance was to be supported. A further requirement was that total beam loss (under fault conditions) should result in a beam trip within one machine pulse, if catastrophic damage to machine components was to be prevented.

A global beam loss monitoring system, using long argon filled ionisation chambers of the Brookhaven [1] type, was considered to be most able to provide the required uniform (and stable) sensitivity per unit beamline length, dynamic range, spatial and temporal resolution, and long term reliability.

## 2 DESCRIPTION

### 2.1 System Overview

The ISIS beam loss monitoring system is composed of three subsystems. This division is dictated by differences in the time dependent nature of beam loss in three distinct machine areas. These are: the 70 MeV $H^-$ linac and transport line; the 800 MeV proton synchrotron; and the 800 MeV proton transport line. A plan view of the global system is shown in Fig. 1. Beam loss in each area is sensed by a linear array of argon filled long ionisation chambers, made from 3 - 4 m lengths of large diameter coaxial cable, and situated 2 - 3 m from the beam axis.

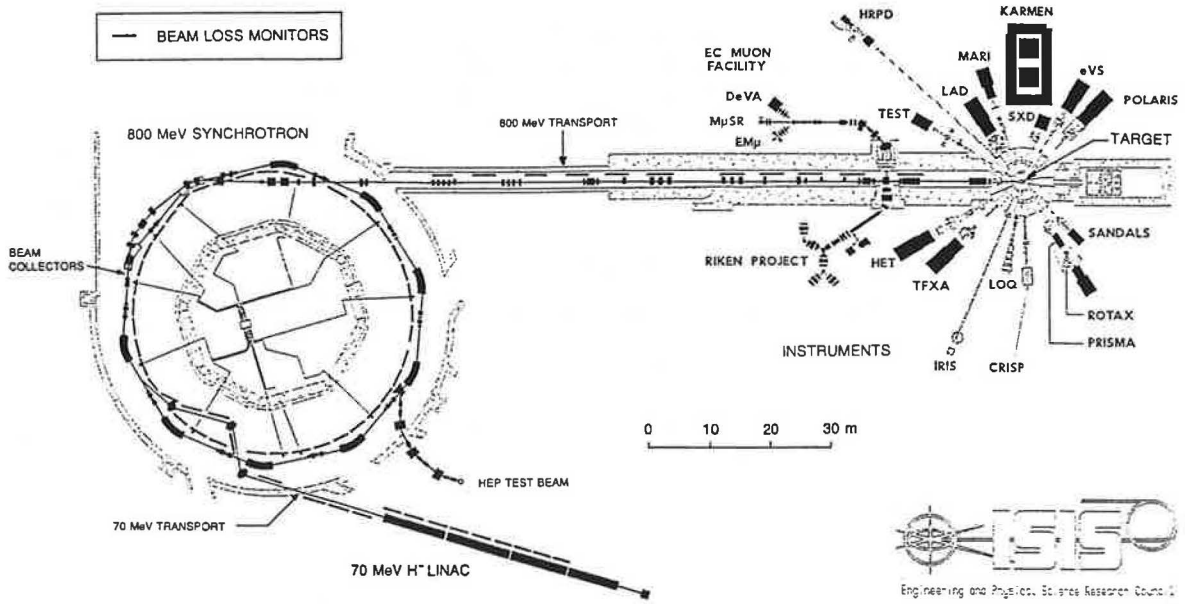


Figure 1: Plan view of ISIS.

## 2.2 *Beam loss detection process*

Mis-directed beam particles ($H^-$ or p) undergo p - n type interactions with the nuclei of machine components (eg. vacuum vessel) to produce forward directed cascade neutrons and isotropically emitted evaporation spectrum neutrons. The latter, after a short flight in air, interact with nuclei in the ionisation chamber wall, to produce the 'knock-on' protons responsible for generating ion-electron pairs in the argon gas, that fills the chamber volume. The ion-electron pairs, separated by the field (10 - 20 V/mm) due to an externally applied bias potential, give the chamber an ideal current source characteristic. Argon filled chambers are used in preference to the simpler air filled option [3], to take advantage of their faster (electron collection) response time, and better saturation characteristics [4,5]. The chambers have good spatial resolution, resulting from the local detection of isotropically emitted neutrons, and, due to their length, do not suffer from the $\frac{1}{r^2}$ dependency shown by point-like radiation detectors.

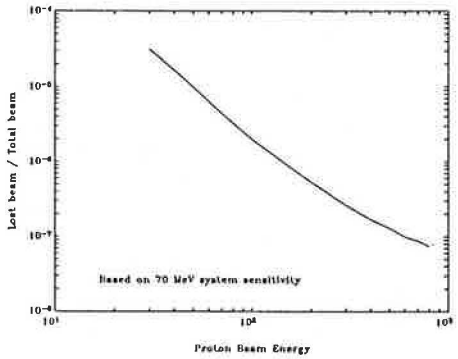


Figure 2: Lower limit of detection.

Ionisation chamber sensitivity to beam loss has been shown to increase rapidly with beam energy in the range 37 - 200 MeV [1], being determined by the neutron yield per incident proton, interacting with a medium atomic number target nucleus [6]. Fig. 2 shows the lower limit of detection for beam loss, as a function of energy, for the ISIS 70 MeV system.

## 2.3 *70 MeV Linac and Transport System.*

The distribution of beam loss monitors (BLM's) in the 70 MeV linac and transport area is shown in Fig. 1. These large diameter (~32 mm), 4 m long monitors have a volume of 2.9 litres, and are pressurised with argon. The monitors, head-amplifiers, cables and gas lines are installed in continuous lengths of protective steel conduit, mounted 2 - 3 m from the beam axis. A cross-section of the standard coaxial termination is shown in Fig. 3. The important features of the signal conditioning and data acquisition system are shown in Fig. 4. A close coupled, low noise, wideband (<.1 Hz - 20kHz) head amplifier boosts the low current ($10^{-7}$ - $10^{-10}$ A), monitor signal and outputs a high level, low impedance differential analogue signal to a

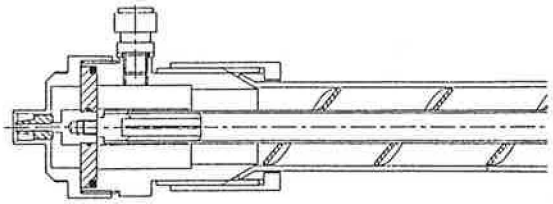

Figure 3: Cross section of BLM (70 MeV system).

remote post-amplifier and data acquisition system. The switched, high voltage bias circuit delivers a ~2 ms charge pulse to the head-amplifier input coupling capacitor during the linac 'dead-time', with a ~0.2 Hz p.r.f. This simple circuit enables a single, low power, supply, to provide very low noise high voltage bias to a distributed set of remote head-amplifiers via a single cable. The high open circuit leakage resistance ($>10^{10}$ Ω) of the high voltage switch, combined with the 0.01 μF input capacitor give an input time constant of T ~ 100 s, in effect providing a ~ d.c. low frequency cutoff, for this a.c. coupled configuration.

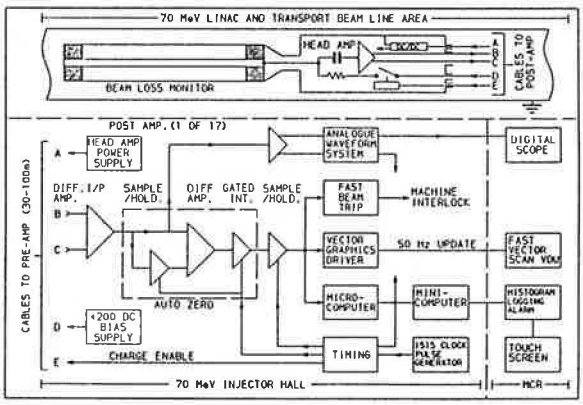


Figure 4: 70 MeV system schematic

Beam loss signals from the linac tank area have a pulsed X-ray background component. These (interfering) flat top pulses, together with head-amplifier zero offset, are rejected by the gated auto-zero circuit in the post-amplifier. As a result, zero drift in the gated integrator is very low.

Analogue signals are output to the analogue waveform system (AWS) and can be selected for display in the main control room (MCR). Loss signals, integrated over the 300 μs linac pulse, update a dedicated vector graphics display in the MCR on a pulse by pulse basis. These signals are also output to a beam interlock unit, and to a data acquisition system that performs a long term logging function.

## 2.4 *800 MeV Synchrotron System*

The distribution of BLM's in the synchrotron is shown in Fig. 1. The monitors are 3 m long, 16 mm in diameter, and have an active volume of 0.6 litres. They are mounted 2 - 3m from the beam axis in free-standing lengths of protective steel conduit, linked in groups of four per super-

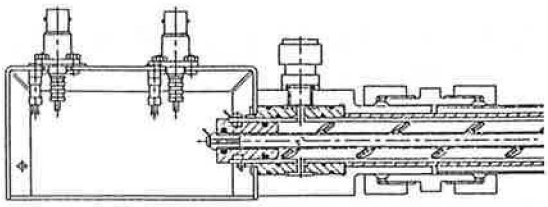

Figure 5: Cross section of BLM (800 MeV system).

period. The necessary degree of radiation hardness, and a dc - 20 kHz frequency response, have been achieved using triaxially configured monitors coupled to remote (~30m) head amplifiers with low capacitance cable. The increasing chamber sensitivity as a function of lost beam energy in the 70 - 800 MeV range (see Fig. 2), and a double-screened installation, help to maintain a good signal to noise ratio. A cross section of the synchrotron BLM is shown in Fig. 5. The important features of the signal conditioning and data acquisition system are shown in Fig. 6. In addi-

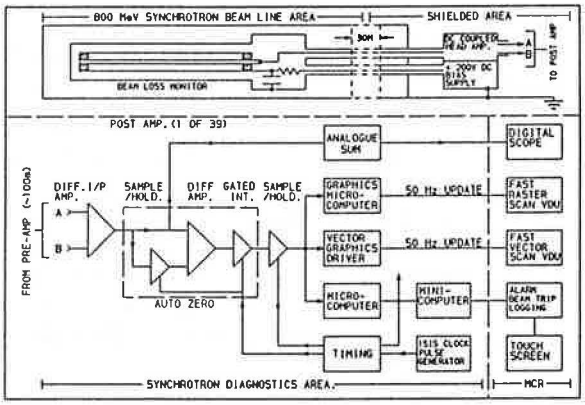


Figure 6: 800 MeV synchrotron system schematic

tion to the facilities provided by the 70 MeV system, this system has two useful tools that aid in minimising beam loss during the 10 ms acceleration cycle. These are; a fast (RISC) microcomputer-controlled display showing beam loss in four preselected time bins, and an analogue sum signal showing total beam loss, in the time domain, on a digitising oscilloscope in the MCR.

### *2.5 800 MeV Transport System*

The distribution of BLM's in this area is shown in Fig.1. The monitors are 4 m long versions of the synchrotron type. Head amplifier time constants have been optimised, to take advantage of the short pulse nature ($<1\mu s$) of the extracted beam pulse. Data is output to a dedicated vector graphics display and to a microcomputer with beam interlock and logging functions.

## 3 OPERATIONAL EXPERIENCE

The global BLM system has proved to be a powerful machine tuning and protection diagnostic. The system plays an important part in ensuring that; operational loss is restricted, almost entirely to 70 - 80 MeV beam, lost during injection (~2%) and trapping (~10%); and that this loss is localised at graphite beam collectors in one superperiod. Dose rates measured 0.5 m from the collectors are typically ~40 mSv/hr, and maintenance in this area requires the use of local shielding and specialised handling methods. Fine tuning techniques, using wideband analogue beam loss signals, have been developed for minimising loss during beam transport, injection, trapping, acceleration and at extraction.

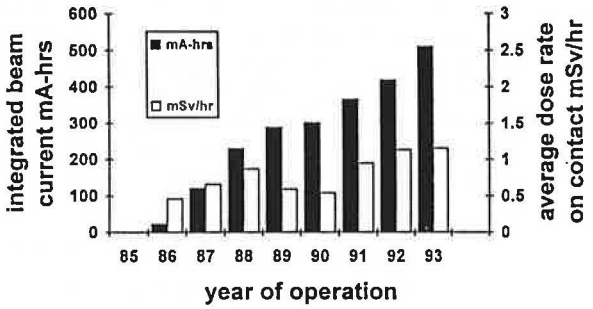


Figure 7: Operational data

Fig. 7 shows yearly totals of beam on target, and also average contact dose rates (excluding loss on collectors) for the synchrotron at the start of the annual shutdown. The data suggests that the regime of 'hands-on' maintenance will continue to be supported with mean beam to target currents in the 180 - 200 $\mu$A range.

## 4 ACKNOWLEDGEMENTS

Thanks are due to G.B.Stapleton (early support), R.L.Witkover (helpful comments), I.S.K.Gardner (analogue sum concept), D.M.Wright (software development), and many others.

## 5 REFERENCES

[1] J.Balsamo, N.M.Fewell, J.D.Klein, R.L.Witkover, "Long Radiation Detector System For Beam Loss Monitoring", IEEE Trans. Nucl. Sci., NS - 24, No. 3, (1977), pp.1807 - 1809.

[2] R.L.Witkover, "Microprocessor Based Beam Loss Monitor System For The AGS", IEEE Trans. Nucl. Sci., NS - 26, No. 3, (1979), pp3313 - 3315.

[3] H.Nakagawa, S.Shibata, S.Hiramatsu, K.Uchino and T.Takashima, "Beam Loss Monitors System With Free-air Ionisation Chambers", Nucl. Instr. and Meth. 174 (1980), pp.401 - 409.

[4] M. Plum, D.Brown, "Response of Air-filled Ion Chambers to High-intensity Radiation Pulses", Proc. 15th Part. Accel. Conf., Washington, Vol. 3, pp2181-3.

[5] J.W.Boag in Radiation Dosimetry. Vol 2, F.H.Attix, W.C.Roesch, Acad. Pr., London, 1966, pp.11 - 27.

[6] H.W.Patterson and R.H.Thomas, Accelerator Health Physics, Academic Press, London, 1973, p.128.

# A Fast Switching E-Field Kicker, For The Temporal and Spatial Division of a 26.6 MeV/c Surface Muon Beam.

M.A.Clarke-Gayther and G.H. Eaton
Rutherford Appleton Laboratory
Chilton, Didcot, UK.

*Abstract*

A description is given of the design and commissioning of a fast switching E-field kicker system, for the temporal and spatial division of a 26.6 MeV/c muon beam. The system is an important component in a recent CEC funded upgrade of the surface muon experimental facility at ISIS, the high intensity neutron source, at the Rutherford Appleton Laboratory, Chilton, Oxfordshire, United Kingdom.

## 1 INTRODUCTION

The ISIS pulsed muon facility as built in 1987 [1], delivered a pair of 82 ns (fwhm) pulses, with a peak to peak separation of 340 ns, to a single experiment area, at a prf of 50 Hz. This double pulse time structure limited the available frequency range for $\mu$SR (muon spin resonance) to discrete frequencies up to a maximum of approximately 10 MHz. This disadvantage was removed in 1989 by the addition of a fast E-field kicker [2] that removed the second muon pulse. The successful operation of this kicker increased the scientific utilisation of the facility at a cost of a factor of two in intensity. This was a tolerable loss, as the majority of experiments typically used only 30% of the available double pulsed muons, being limited by high data acquisition rates at early times with the consequent severe distortions induced in the measured spectra.

With a single experiment area, there was a three-fold over-subscription for beam time. To solve this problem, a proposal was made in 1989, to the CEC large facilities program, to extend the facility, and provide three experiment areas with the capability of simultaneous operation with single pulses at a prf of 50 Hz. This was to be achieved with a temporal and spatial division of the muon pulse pair by a fast switching E-field septum kicker.

## 2 MODE OF OPERATION

A plan view of the CEC funded muon beam line is shown in Fig. 1, with the position of the kicker indicated by the letter K. Operation of the CEC kicker is illustrated in Fig. 2. A simplified plan view shows the 700mm long central anode, equidistant from the two outer grounded cathodes. At the start of the cycle, the central anode is at a potential of 32.5 kV, producing an electric field of about 0.6 MV/m in the gaps. The first muon bunch is bisected and subsequently deflected through angles of 66.5 mr by

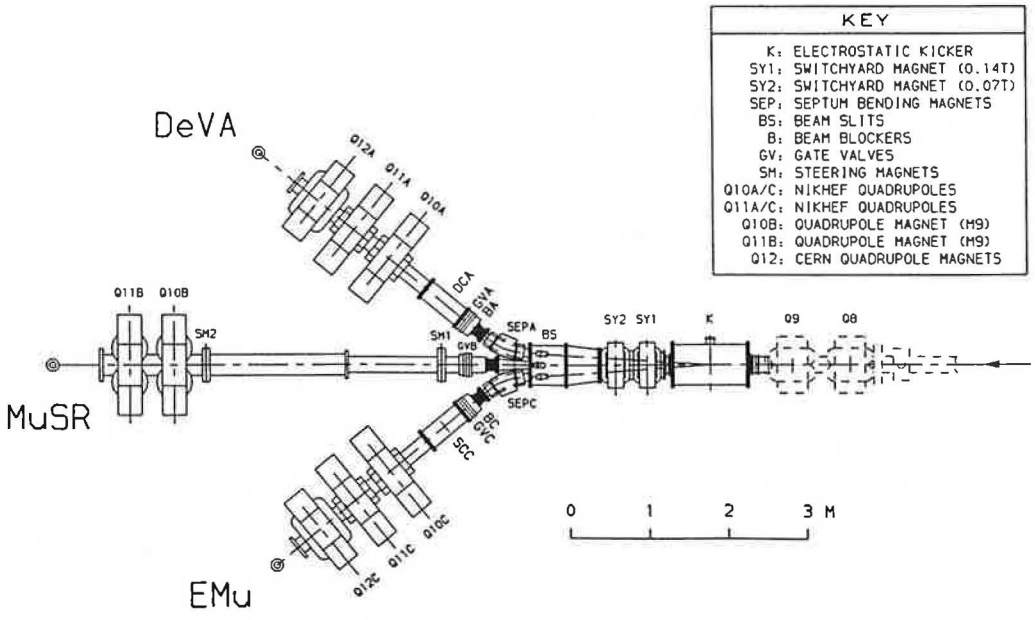


Figure 1: Plan view of the CEC muon beam lines

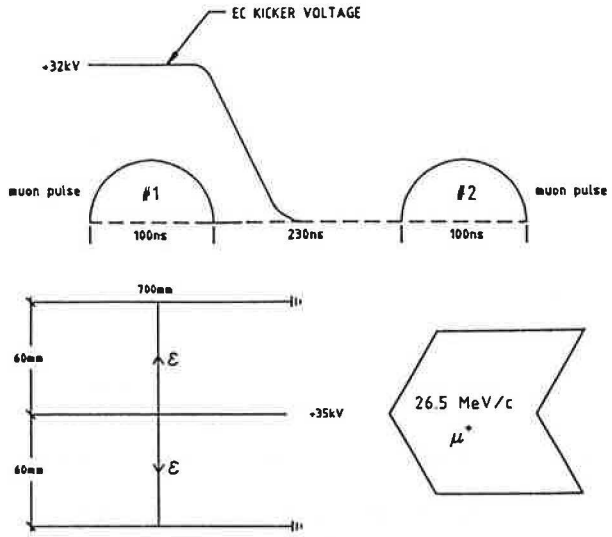


Figure 2: Mode of operation

the electric field, to provide two simultaneous muon pulses to the outer (EMu and DeVA) areas. Just after the passage of the first muon pulse the kicker field is rapidly reduced to zero. The second muon pulse is consequently undeflected, and travels on to the MuSR area.

## 3 MECHANICAL CONSTRUCTION OF THE CEC KICKER

The mechanical construction of the E field kicker is shown in Fig. 3. This design produces the required 66.5 milliradian deflection, for 26.61 MeV/c positive muons, with an electrical length of 0.7 metres, and an applied voltage of 32.5 kV.

Maximum deflection for a given electrical length, and applied voltage, has been achieved by matching the curvature of the outer electrodes to the path of the deflected muons. The finite element code PE2D [3] was used to model and optimise the electric field design.

Components subject to high electric fields are manufactured from 304 grade stainless steel, and have been electropolished to achieve a suitable surface finish [4]. The selection of a 2.0 mm thick central electrode was dictated by the need to maintain adequate stiffness and flatness, a field level of not more than 50 kV/cm at the fully radiused electrode edge, and minimum muon loss (~5%).

Other features of the design are the commercial high voltage feedthrough, the use of canted beryllium/copper spring rings, and fingerstrip to provide low impedance electrical connections between the 'in vacuum' components. The high voltage electrode support insulators are made from 'PEEK' [5], a strong, high temperature, advanced polymer, and have been designed using specialised techniques [6].

## 4 THE CEC KICKER DRIVE SYSTEM.

A block diagram of the kicker system is shown in Fig. 4. This low power configuration is capable of charging the kicker electrode to 32.5 kV (±0.25%) in less than 15 ms, and discharging to 0 V (±0.25% of 32.5 kV) in less than 200 ns.

The CX1528 medium power, single gap thyratron [7], was selected for its good high voltage holdoff, convenient air cooling, and the promise of a long operational life in this application.

Other features of the design are the commercial high voltage capacitor charging supply with internal gating function, stabilised DC heater and reservoir supplies (for reduced thyratron trigger jitter), and a commercial high voltage power mosfet thyratron trigger unit.

A timing waveform schematic is shown in Fig. 5. At t=0, V2 has settled to 32.5 kV (±0.25%), and the thyratron grid driver has just received a trigger pulse. At t=150 ns the first muon pulse enters the kicker, and is horizontally divided and deflected through equal and opposite angles of 66.6 mrad, by the electric field. These muons are subsequently transported through a septum magnet to the

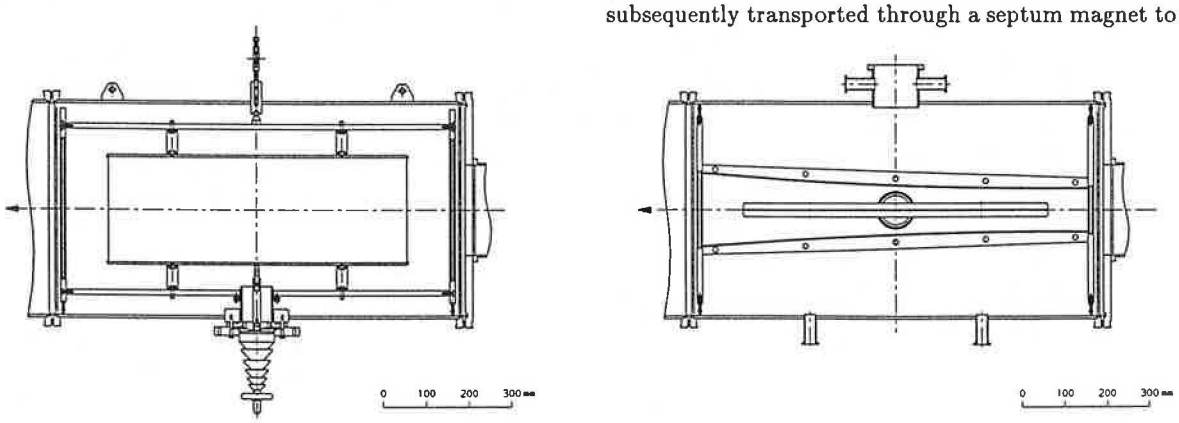


Figure 3: CEC kicker showing side and plan views

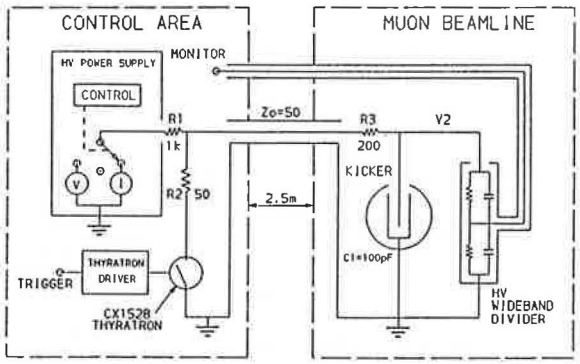


Figure 4: Block diagram of the CEC kicker system

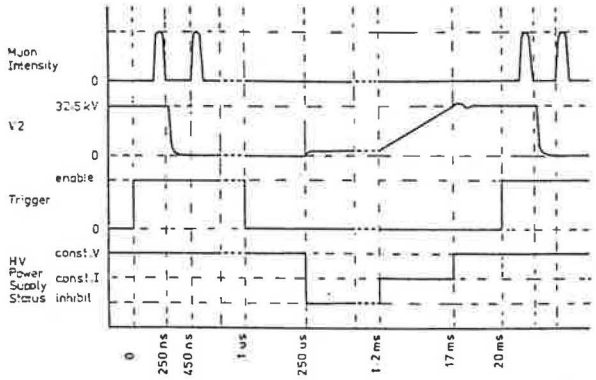


Figure 5: Timing and waveform schematic

left and right experimental areas. At t=250 ns, the thyratron fires, and V2 decays with a time constant of C1*(R2+R3) (25 ns). The timing is set so that at t=250 ns the first muon pulse has (just) passed through the kicker. At t=450 ns the second muon pulse enters the kicker and passes through, undeflected, to the central experimental area. At t=250 $\mu$s the high voltage power supply responds to the low impedance load at its output, and switches from constant voltage to inhibited mode. After an internally generated delay of about 1 ms, the supply switches to constant current enabled mode (t=1.2 ms). At t=17 ms, the system capacitance (500 pF) is charged to 32.5 kV, and settles to 0.25% of 32.5 kV by t=19.5 ms, ready for the next cycle.

## 5 OPERATIONAL MEASUREMENTS

At the time of writing, the kicker system has run with beam for more than 4500 hours, with few problems. The operating voltage, predicted by electrostatic field computation [3] of 32.0 kV compares favourably with that obtained by the optimisation of muon intensity in the DeVA and EMu beam lines (32.5 kV). The voltage waveform, measured with a wide-band high voltage probe (Tek P6015A), shows the voltage settling to $< 0.25\%$ of 32.5 kV in 180 ns.

Fig. 6 shows the action of the CEC kicker on the muon

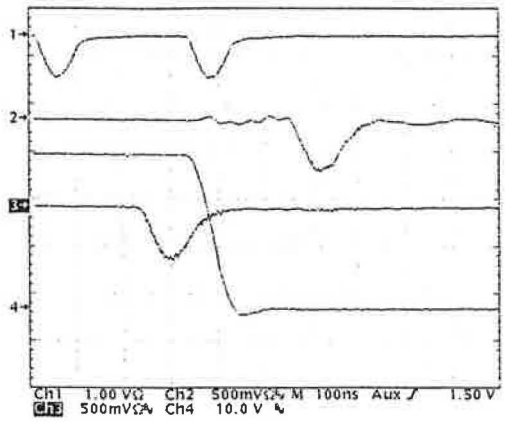


Figure 6: Action of CEC kicker on muon pulses

pulses. The top trace shows the Cerenkov pulses revealing the time structure of the protons at the production target. The second and fourth traces are derived from the muon detectors in the MuSR and EMu beam lines respectively, and show the relationship with the kicker voltage waveform (third trace) in distributing the two muon pulses to the EMu/DEVA and MuSR beam lines.

## 6 ACKNOWLEDGEMENTS

Thanks are due to D.J.McPhail (mechanical design), M.Krendler (alignment), T.P.Parry (vacuum), C.D.Uden (engineering administration), C.A.Scott (helpful discussions), W.G.Williams (project coordinator), and many others.

## 7 REFERENCES

[1] G.H.Eaton, A.Carne, S.F.J.Cox, J.D.Davies, R.De Renzi, O.Hartmann, A.Kratzer, C.Ristori, C.A.Scott, G.C.Stirling and T.Sundqvist. Nuclear Inst. and Meth. A269(1988) p.453.

[2] A.I.Borden, A.Carne, M.A.Clarke-Gayther, G.H. Eaton, H.J.Jones, G.Thomas, D.Hartmann and T. Sundqvist. Nucl. Inst. and Meth. A292(1990) p.21

[3] PE2D "A two dimensional static and time varying field computational package." Vector Fields Ltd, 24 Bankside, Kidlington, Oxford OX5 1JE

[4] F.McCoy, C.Coenraads, M.Thayer, "Some effects of electrode metallurgy and field emission on high voltage insulation strength in vacuum", Proc. of the First Int. Symp. on Insulation of high voltages in vacuum, MIT, USA, Oct. 1964, Addenda No. 1

[5] PEEK Polyaryletherketone, ICI Materials, PO Box 90, Wilton, Middlesborough, Cleveland TS6 8JE, England

[6] J.P.Shannon, S.F.Philp, J.G.Trump, "Insulation of high voltage across solid insulators in vacuum", Proc. of the First Int. Symp. on Insulation of high voltages in vacuum, MIT, USA, Oct. 1964, p.281 - 304

[7] English Electric Valve Company Ltd, Waterhouse Lane, Chelmsford, Essex, CM1 2QU

# DIGITAL CONTROL SYSTEM FOR THE ISIS SYNCHROTRON MAIN MAGNET POWER SUPPLY

M. GLOVER, W.EVANS, G. MARTIN, W. MORRIS
ISIS Facility, Rutherford Appleton Laboratory, Chilton, Didcot, Oxon., 0X11 0QX, England

*Abstract*

The main magnet power supply control system of the ISIS 800 MeV rapid-cycling proton synchrotron is described. With the machine currently operating with beam intensities in excess of 185 μA, acceptable performance is dependent on the stability of the main magnet power supply, and the performance of the closed loop systems used to control the supplies.

## 1. INTRODUCTION

On the ISIS synchrotron the dipoles, doublet quadrupoles and singlet quadrupole magnets are connected in series using a configuration known as a "White" circuit, see Fig 1. This circuit is resonated at the operating frequency of 50 Hz to reduce the reactive load on the make up supply. It also has the advantage of ensuring that the same current, (leakage current excepted), flows in all the magnets. A DC supply is used to bias the sinusoidal magnet waveform . This has the advantage of increasing the efficiency of the White circuit by reducing the total power requirement for the same change in magnetic field from injection to peak energy. The DC bias is connected by splitting and centre-grounding one element of the White circuit . For further information on the White circuit see [1].

The AC make up power supply is supplied to the primary of the White circuit , and the digital control system is used to ensure that the stability of the system is better than 1:1000 of the set value.

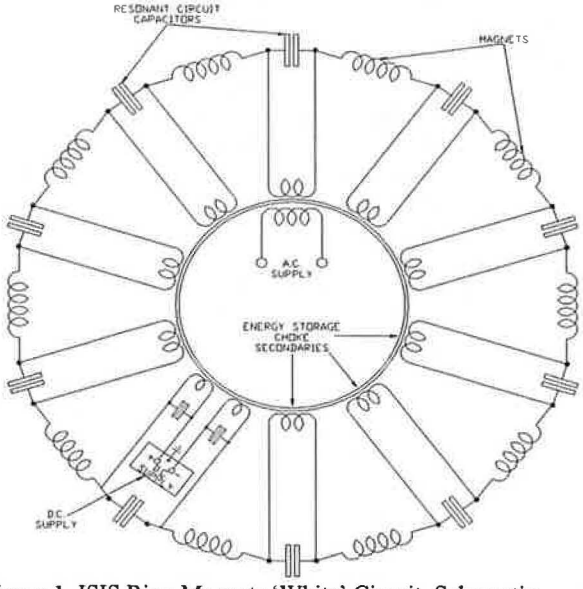


Figure 1. ISIS Ring Magnets 'White' Circuit Schematic

## 2. A.C. SYSTEM

### *2.1 A.C. Make Up Power Supply*

The ISIS A.C. make up power supply consists of an A.C. single phase generator driven by a variable drive D.C. motor using a resilient coupling. The A.C. generator used has been converted to single phase from a three phase 50 Hz generator. The required drive to the D.C. motor is via two 400 kW A.C. to D.C. converters coupled in series. A variable voltage alternator rotor excitation supply, which is directly coupled to the rotor slip rings is then used to control the amplitude of the A.C. . A schematic diagram of this arrangement is shown in Fig 2.

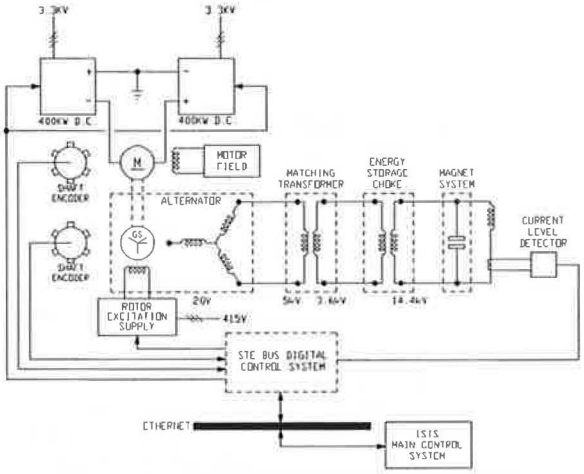


Figure 2. ISIS A.C. Make Up Power Supply

Control of the A.C. make up supply is via a system which utilises two separate closed loop systems to effect accurate control of the A.C. magnet phase and amplitude .

### *2.2 Single Phase A.C. Generator*

The alternator used was originally a three phase 50 Hz generator. To enable it to be used as a 50 Hz single phase source the following modifications have taken place. The stator has been fitted with magnetic slot wedges, and copper plates and connecting rings have been fitted to the rotor pole tips.

These modifications have been undertaken to reduce the pole flux to a minimum. Without these alterations the resultant pole flux will produce at twice the operating frequency large losses in the rotor magnetic circuit, and induce high voltages in the field windings. The theory of A.C. generators and modifications for single phase use can be further studied in

[2]. Even with these alterations the remaining flux reacts with the excitation winding, generating a 100 Hz pulsating emf. (see Fig 3.). This emf. is superimposed upon the direct voltage output of the excitation supply. Therefore the rotor excitation supply used must be capable of withstanding a ripple current of approximately 20 Amps . Also any control system used for the amplitude control of the A.C. must also take this into consideration.

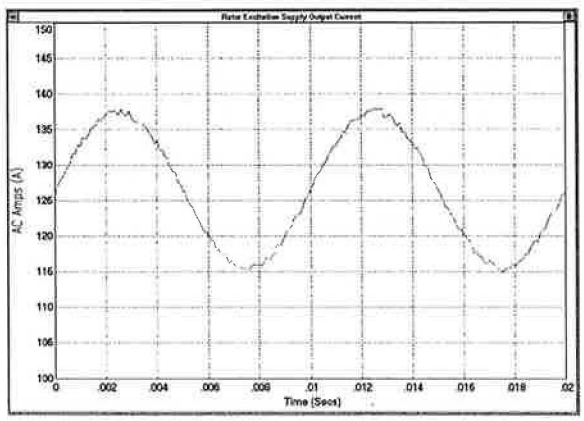


Fig 3. Alternator Rotor Excitation Supply Output Current

## 3. CONTROL SYSTEM

### *3.1 System Configuration*

The control system consists of an STEbus IEEE1000 system using a Motorola 68000 16 MHz microprocessor, running 0S-9 real time operating system. The schematic of the system is shown in Fig 4.

STEbus was already in use for other microprocessor based systems on ISIS. This combined with the wide range of commercially available I/O and signal conditioning boards from a multitude of companies meant that , STEbus was an ideal and cost effective choice for the system.

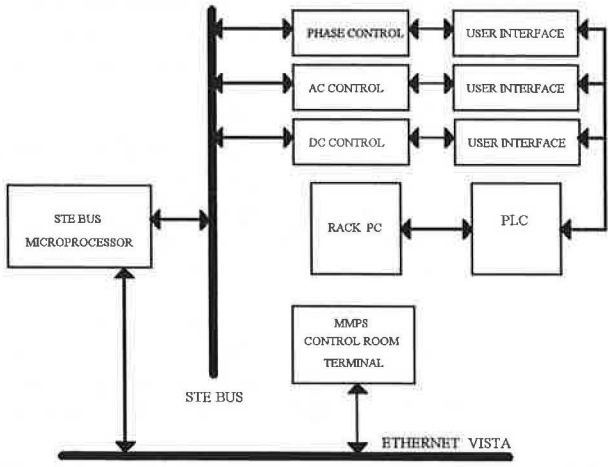


Figure 4. MMPS Digital Control System Schematic

The control system is required to provide a high degree of stability in an environment which includes rotating plant, magnetic fields , large power supplies and electric cooling fans. It is therefore safe to assume that any form of signal interference that can be thought of will be present, and must be eliminated from the control signals. Noise reduction techniques such as signal isolation , differential signals , shielded cables, signal ground and ground loop considerations, signal filtering and cable locations were all employed. There was no point in building a control system for 16 bit performance if the control signals picked up 50 mV of noise on their way to the power supply.

### *3.2 OS-9 Operating System*

OS-9 is a multi-tasking real time operating system which was originally developed for the Motorola range of microprocessors. This means that as it was developed for the 68000 range , it can make optimum use of the devices capabilities such as interrupts, whilst optimising the code required in terms of code size and speed.

The interrupt driven aspect of the software means that code for updating the screen display, communicating with the user or ethernet, and dealing with interlocks need only be run when required. This allows the microprocessor to concentrate on the PID software loops for the phase and amplitude control of the A.C. waveform.

The real benefit from using OS-9 comes from its ability to multi task programs on a time sliced real time prioritised basis. These priorities determine the amount of CPU time allowed for a program and can be changed by the user or by the software itself. The software for sampling the feedback signals also uses the OS-9 feature of 'cyclic alarm'. These ensure that the signal sampling interval is fixed on a periodic time interval determined by the user. Further technical details of OS-9 can be found in [3] .

### *3.3 Phase Control*

Phase control of the A.C. waveform is obtained by phase locking the feedback signal of a shaft encoder to a master oscillator. This control of the phase is performed in two stages. First the D.C. motor is run up to its normal 1000 rpm operating speed . When the motor has stabilised, the phase of the shaft encoder signal is compared with the phase of the master oscillator signal by a class 2 phase comparator on a phase locked loop IC. The output of the voltage controlled oscillator section of the PLL is then converted into a 16 bit digital representation of the phase difference.

This digital phase difference is then used as the error signal into the phase PID software loop. The demand to the converters which power the motor is then adjusted by the PID loop . This ensures that the phase of the A.C. waveform does not vary by +/- 0.25 Hz and is locked to the master oscillator.

The shaft encoders are free floating so that they survive any end thrust of the shaft due to magnetic centre off-set at motor start up and stop. Two encoders are located on the

shaft , at the motor and alternator respectively. This is in case of failure of the selected encoder, but it also allows us to measure the degree of rotational twist in the motor alternator shaft.

*3.4 Amplitude Control*

The feedback signal for the amplitude control is derived from a direct current current transducer (DCCT), which is located in the magnet current line of one of the super-period elements of the ISIS 'White' circuit. This composite magnet current signal is filtered to extract the A.C. component, which is used as the error signal.

This error signal which is a 50 Hz sine wave is converted into a dc level representing the peak amplitude of the A.C. magnet current, by a peak detector and a 16 bit resolution sample and hold circuit. This circuit is refreshed at 50 Hz to ensure that a valid peak A.C. value is always seen by the PID software . See Fig 5.

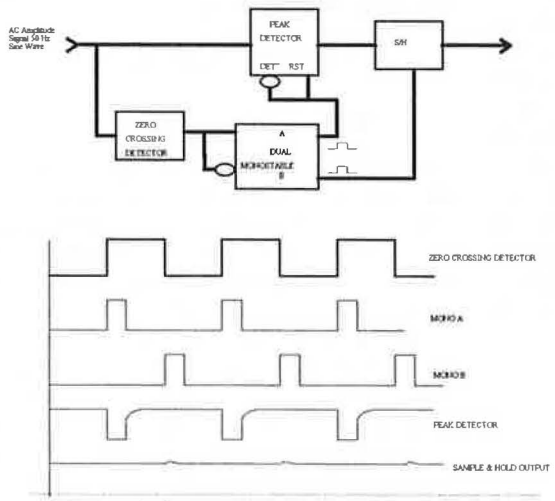


Fig 5. A.C. Amplitude Error Signal Generation.

The resonant magnet network has low intrinsic damping and excessive corrections by the PID loop to the amplitude of the A.C. can cause overshoot and subsequent damped oscillations. For this reason and to limit the effect of any noise on the error signal, the response of the PID loop is limited to a maximum error that it can correct.

## 4. SOFTWARE

*4.1 General Software*

The software is written in a modular format so that each block deals with a different aspect of the control system. This is to make full use of the multi-tasking interrupt driven aspect of the OS-9 operating system.

Each module is capable of operating as a stand alone program and has been written so that it does not interfere with the PID control loop software modules. The separate modules are linked via a common data module which is used to pass data from one module to another and for updating the screen displays.

*4.2 PID Loops*

The algorithm of a proportional + integral + derivative (PID) controller is shown below (Fig 6), along with its block diagram implementation. This use of a software PID system allows the user to tune the system whilst the plant is in operation.

$$c(t) = \frac{1}{Kp}\left[e(t) + \frac{1}{Ti}\int e\ d(t) + Td\left[\frac{de}{dt}\right]\right]$$

Steady State Gain = 1/Kp . System Error = e(t)

Intergral Action Time = Ti . Derivative Action Time = Td

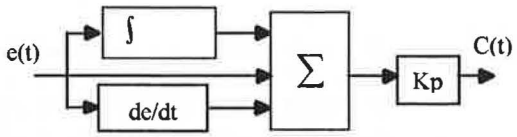


Figure 6. PID Algorithm & Block Schematic

The software version also allows coefficient settings that would be extremely difficult to implement accurately with discrete components on an analogue controller. These coefficients can be adjusted independently which is not always the case with the analogue version.

The nature of a software PID controller implies the use of sampled data. This has both advantages and disadvantages. The sampled data can be filtered to remove any noise or false readings before it enters the controller. However sampled data integration implies an approximation due to the non time continuous nature of the data. This subsequently introduces an error. The higher the order and complexity the integration algorithm is the smaller the error, but the CPU takes longer to compute the result. The integration algorithm used was selected on a trial and error basis of finding the simplest and lowest order which gave the required accuracy.

Another advantage of using a PID software module is that the separate blocks can easily be reconfigured to reduce certain types of system responses. Sensitive control to system fluctuations, but smooth changes to set point changes can be achieved by removing the deriative action from the set point . This reconfigures the controller into a IP-D system.

## 5. REFERENCES


[1] W. Bothe, Resonant Excitation of Synchrotron Magnets, in Proceedings of Power Converters for Particle Accelerators, Montreux, Switzerland, March 1990, pp 271 - 303.

[2] J.H. Walker, Large Synchronous Machines, Oxford: Oxford Science Publications, 1981, pp 232 - 237.

[3] Microware Systems Corp., 0S-9 Manual ver 2.4, Des Moines, Iowa, March 1991.

# Low Intensity and Injection Studies on the ISIS Synchrotron.

C M Warsop,
Rutherford Appleton Laboratory,
Chilton, Didcot, Oxon, England.

*Abstract.*

Recent diagnostic work on the 800 MeV, High Intensity Proton Synchrotron of ISIS, the Spallation Neutron Source at RAL, is presented. The use of a beam 'chopper' to provide very short injected pulses, 0.1% of normal intensity, for machine studies is described. The measurements made possible with these 'chopped' beams, their application in optimising the machine, and the techniques employed are reported.

## 1. INTRODUCTION.

The ISIS Synchrotron accelerates $2.5 \times 10^{13}$ protons per pulse, at 50 Hz, from 70 to 800 MeV. At normal operating intensities, a large fraction of the available transverse and longitudinal acceptances of the machine are occupied by beam. As a result, measurements are limited to averages over large beams; any detailed information on motion within the beam is not obtainable. This is a basic problem in studying high intensity machines. However, it is possible to study motion of low intensity beams which fill a small fraction of the machine acceptances. In doing so, all high intensity effects are lost, but a great deal of information on the precise set up of the machine, and properties of the injected beam are made available.

## 2. INJECTION PROCESS AND BEAM 'CHOPPER'.

### *2.1 Injection Process.*

The high intensity beam is established in the ISIS synchrotron using $H^-$ multi-turn, charge-exchange injection. During the injection process (200 $\mu$s, 130 beam revolutions), the sinusoidal fields in the main lattice magnets fall, and separately programmed trim quadrupoles are used to correct for chromatic effects. This keeps the constant energy injected beam away from resonances. The transverse phase spaces of the synchrotron are 'painted' such that space charge effects are minimised. Horizontally beam is injected at a fixed point, and movement of the closed orbit caused by the falling magnet fields provides a suitable spread in betatron amplitudes. Vertically, the injection point is moved about the stationary closed orbit with a programmable steering magnet in the injection line, to similar effect. Optimising momentum spread of the injected beam is also important. The number of changing parameters, and the importance of precise injection set-up for high intensity running, means that ability to make detailed measurement of the process is extremely useful.

### *2.2 Beam 'Chopper'*

On ISIS, an appropriate 'diagnostic' beam is obtained by using an electrostatic kicker or 'chopper' in the injection beam line, which allows pulse lengths of down to 100 ns to be injected. This occupies a fraction of the circumference (revolution time at injection is 1.48 $\mu$s) and so allows studies of longitudinal motion. The injected beam has transverse emittances of 25 $\pi$ mm-mr and occupies a small fraction of the synchrotron acceptances ($\sim$500 $\pi$ mm-mr), which allows motion in transverse planes to be easily observed. With appropriate diagnostic techniques these 'chopped beams' have become a powerful tool for accurately measuring and specifying machine set-up.

## 3. TRANSVERSE MEASUREMENTS.

### *3.1 Method.*

The technique and some applications of transverse measurements have been covered in a previous paper [1]. This work will be briefly reviewed and updated here.

A 600 ns chopped beam is injected, and the transverse position of its centroid monitored at a single machine azimuth over about 40 successive turns. Signals from an electrostatic pick-up are digitised and processed on a PC. The 'sampled' betatron oscillation measured on each turn, is modified by (i) the changing lattice magnet fields and (ii) the finite spread in betatron frequencies. The former leads to a slow change in frequency and other characteristics of the oscillation, whilst the latter causes a relatively fast 'damping' of the measured centroid motion. A theoretical function (1) for the positions on each turn can be derived [2], and by least squares fitting of the measured positions to this, accurate estimates of many key parameters can be obtained.

$$y_n = A \cdot \exp\left(-\frac{(\pi \cdot n \cdot \delta Q)^2}{2}\right) \times \cos\left(2\pi \cdot n\left[Q_0 + \frac{n \cdot \Delta Q}{2}\right] + 2\pi \cdot \phi\right) + n \cdot \Delta R + R_0 \quad (1)$$

where $y_n$ - position on $n^{th}$ turn,
A - initial betatron amplitude,
$Q_0$- initial Q value,
$R_0$- initial closed orbit,
$\delta Q$- Q spread,
$\phi$ - initial betatron phase/$2\pi$,
$\Delta Q$- change in Q per turn.,
$\Delta R$- change in R per turn.

### 3.2 *Measurements.*

*(i) Specifying Operational Injection Set Up.*

Injecting chopped beams at different times and fitting the function (1) to measured beam positions, as described, one can determine the time variation of parameters. The change of betatron amplitude and closed orbit through the injection period show how the transverse phase spaces are being painted. Typical, empirically optimised values for high intensity are shown in Figure 1. Q values are also determined by these measurements and give a useful indication of machine set-up.

Figure 1: Variation of Key Parameters Through Injection.

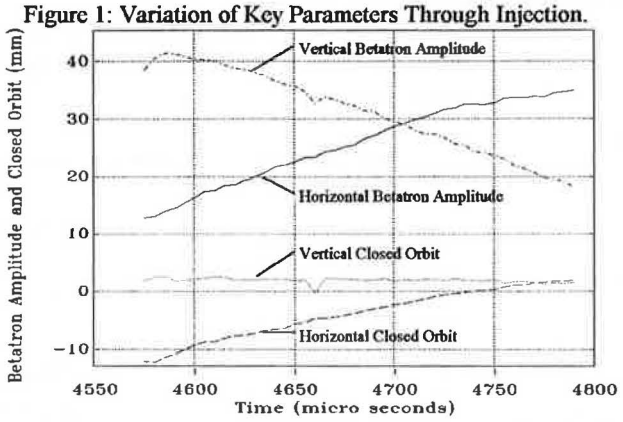


The beam is chopped once in every 128 of the 50 Hz pulses; interleaved high intensity pulses are unaffected. The resultant loss in user beam (<1%) is acceptable and so allows many measurements during operational running. Many machine parameters can be pulsed to experimental values for the chopped pulse, which has expanded the scope for on-line experiment considerably.

*(ii) Q Value and Chromaticity Measurements.*

The accurate measurement of Q values ($\pm 0.002$) has allowed checks on the lattice, the operation of the trim quadrupoles, and optimum correction of Q to avoid resonances. The change in Q of the constant energy chopped beam with changing main magnet field through injection (trim quads off) yields values of chromaticity. On ISIS the relation $\Delta Q/Q$ vs $[\Delta B/B]_p$ is highly linear, both $\xi_h$ and $\xi_v$ are $-1.4 \pm 0.1$.

*(iii) Beta Function Measurements.*

The variation of Q with current in a quadrupole gives a measurement of the synchrotron beta function - at the quadrupole. From [3]

$$\Delta Q \approx \frac{1}{4\pi}\int \Delta k \cdot \beta(s) \cdot ds \approx \frac{\bar{\beta} \cdot S}{4\pi} \cdot \frac{e}{P} \cdot G \cdot \Delta I \quad (2)$$

where all notation is standard except: G - gradient/amp, $\bar{\beta}$ - mean beta over quad length S. The gradient of the approximately linear relation $\Delta Q$ vs $\Delta I$ thus measures beta.

The ISIS Synchrotron consists of 10 superperiods, each with 2 independently programmable trim quadrupoles, where beta may be measured. This method depends on the accurate measurement of Q, as allowed by chopped beams. Variation of beta around the machine at equivalent lattice positions, and comparison of absolute values with theory, has given valuable information on the machine.

*(iv) Betatron Phase Advances.*

Simultaneous measurements at many monitors around the ring, would give azimuthal variation of $\phi$ in (1), and thus the phase advance between monitors. On ISIS, limited number of digitising channels available, and inappropriate electronics on most monitors (optimised for high intensity) have made such measurements difficult. However, measured phase advances ($\phi$) between monitors, agreed in most cases with theoretical values to within the estimated accuracy of $\pm 0.02$.

## 4. LONGITUDINAL MEASUREMENTS.

### 4.1 *Longitudinal Beam Structure at Injection.*

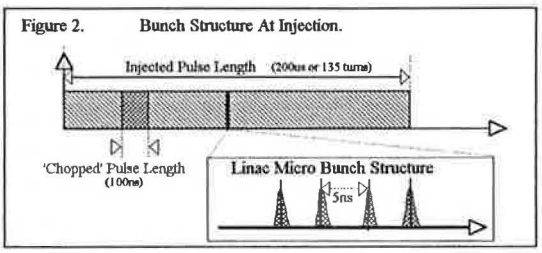


The 202.5 MHz linac provides a 200 $\mu$s macro pulse length, composed of 1 ns micro-bunches, spaced by 5 ns. These debunch while drifting over 35.8 m, to a sinusiodally excited debuncher cavity, which is used to optimise momentum spread for the synchrotron. Particles then drift 16 m to the stripping foil where they enter the synchrotron.

Figure 3: Typical Debunching Profile.

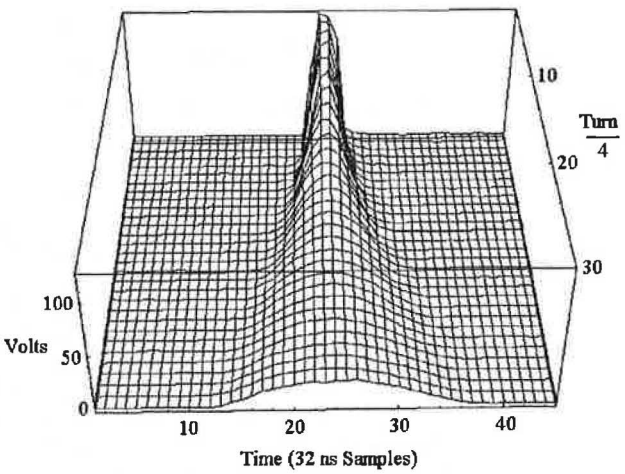

*4.2 Measurement of Injected Momentum Spread.*

The 200 $\mu$s injection macro pulse is chopped to 100 ns. This pulse consists of 20 micro-bunches, which merge in the first few turns in the synchrotron. The 20 micro-bunches will, *on the first turn*, have just started to run into one another. The periodic structure resulting approximates to a uniform momentum distribution with time. This assumption allows a fairly simple treatment for deconvoluting the momentum spread.

Longitudinal profiles are obtained from an electrostatic pickup. Digitising chopped beam signals over 100 turns, with RF off, gives the debunching profile as in Figure 3. From this momentum spread can be obtained as follows.

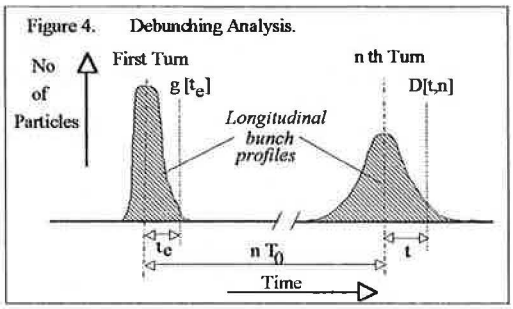


A particle starting at time $t_e$ relative to the bunch centre on the first turn (Figure 4), will arrive at time t on the $n^{th}$ turn if $\Delta T$, the change in revolution time per turn due to momentum error, is such that:

$$t = t_e + n \cdot \Delta T \quad (3)$$

From the definition of $\eta$

$$\Delta T = \frac{\eta \cdot (P - P_0)}{P_0} \cdot T_0 \quad (4)$$

Let $g[t_e]$ be the bunch profile on the first turn, and $f[\Delta P/P]$ the normalised momentum distribution of the bunch, which is assumed to be uniform with time *on the first turn*. The number of particles arriving at time t, from those starting at time $t_e$, is given by:

$$d[t, t_e] = g[t_e] \cdot f\left[\frac{P_e - P_0}{P_0}\right] \quad (5)$$

where $P_e$ is defined by (3) and (4), so that:

$$\frac{P_e - P_0}{P_0} = \frac{t - t_e}{n \cdot \eta \cdot T_0} \quad (6)$$

Substituting into (5), and integrating over the profile on the first turn, gives the profile on the $n^{th}$ turn D[t,n].

$$D[t,n] = \int d[t, t_e] \cdot dt_e = \int g[t_e] \cdot f\left[\frac{(t - t_e)}{n \cdot \eta \cdot T_0}\right] \cdot dt_e \quad (7)$$

This is a convolution of the function $g[t_e]$ on $f[\Delta P/P]$. The debunching profile over ~100 turns gives $g[t_e]$ and D[t,n] for many n. A numerical deconvolution of $g[t_e]$ into D[t,n] yields the function $f[\Delta P/P]$, the momentum distribution. The numerical algorithm used is described in [4].

The simplest method involves a process identical to polynomial long division, but has a tendency to be unstable. However, with suitable local smoothing, good results can be obtained. More sophisticated numerical methods are presently being considered.

*4.3 Application.*

The above method allows routine measurement of injected momentum spreads during operational running, throughout the injected pulse. Usual operational values of 95% full width in fractional momentum spread, are about $4.5 \times 10^{-3}$, with typical scatters being $\pm 0.2 \times 10^{-3}$. Measured momentum spread distributions, as a function of debuncher setting are shown in Figure 5. The effect of the debuncher is clearly demonstrated.

Figure 5.

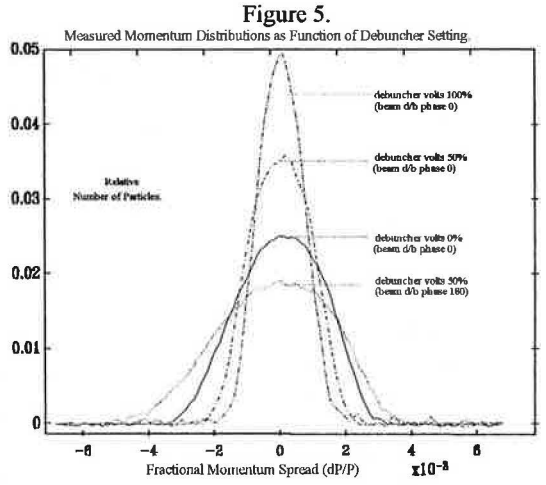


## 5. CONCLUSIONS.

The use of very low intensity chopped beams on the ISIS synchrotron has allowed much detailed and accurate measurement, not really possible in any other way.

## 6. ACKNOWLEDGEMENTS.

The author would like to acknowledge the help and advice of A I Borden, I S K Gardner, M R Harold, G H Rees and C W Planner during the course of this work. Thanks are also due to the ISIS Crew, D J Adams and H Zhang.

## 7. REFERENCES.

[1] C M Warsop, 'Low Intensity and Injection Studies on the ISIS Synchrotron'; Proceedings of ICANS XII, May 1993, RAL Report RAL 94-25.

[2] L Ahrens *et al.*, 'A Method for Determining the Position, Angle and other Injection Parameters of Short Pulsed Beams in the AGS'; IEEE Tr Nu Sci Vol. NS-32, No 5 Oct 1985.

[3] Courant and Snyder, Ann. Phys. 3 (1958).

[4] R N Bracewell, 'The Fourier Transform and Its Applications', McGraw-Hill.